SCIENCE CHINA
Earth Sciences

• REVIEW •

July 2012 Vol.55 No.7: 1052–1078
doi: 10.1007/s11430-012-4444-x

Progresses on microwave remote sensing of land surface parameters

SHI JianCheng[1*], DU Yang[2], DU JinYang[1], JIANG LingMei[3], CHAI LinNa[3], MAO KeBiao[4], XU Peng[5], NI WenJian[1], XIONG Chuan[1], LIU Qiang[1], LIU ChenZhou[1], GUO Peng[1], CUI Qian[1], LI YunQing[1], CHEN Jing[5], WANG AnQi[6], LUO HeJia[2] & WANG YinHui[2]

[1]*State Key Laboratory of Remote Sensing Science, Jointly Sponsored by the Institute of Remote Sensing Applications of Chinese Academy of Sciences and Beijing Normal University, Beijing 100101, China;*
[2]*Department of Information Science and Electronic Engineering, Zhejiang University, Hangzhou 310058, China;*
[3]*State Key Laboratory of Remote Sensing Science, Jointly Sponsored by Beijing Normal University and the Institute of Remote Sensing Applications of Chinese Academy of Sciences, Beijing 100875, China;*
[4]*Institute of Agricultural Resources and Regional Planning, Beijing 100081, China;*
[5]*School of Remote Sensing and Information Engineering, Wuhan University, Wuhan 430072, China;*
[6]*Base of the State Laboratory of Urban Environmental Processes and Digital Modeling, Capital Normal University, Beijing 100048, China*

Received February 6, 2012; accepted May 2, 2012

Highly accurate observations at various scales on the land surface are urgently needed for the studies of many areas, such as hydrology, meteorology, and agriculture. With the rapid development of remote sensing techniques, remote sensing has had the capacity of monitoring many factors of the Earth's land surface. Especially, the space-borne microwave remote sensing systems have been widely used in the quantitative monitoring of global snow, soil moisture, and vegetation parameters with their all-weather, all-time observation capabilities and their sensitivities to the characteristics of land surface factors. Based on the electromagnetic theories and microwave radiative transfer equations, researchers have achieved great successes in the microwave remote sensing studies for different sensors in recent years. This article has systematically reviewed the progresses on five research areas including microwave theoretical modeling, microwave inversion on soil moisture, snow, vegetation and land surface temperatures. Through the further enrichment of remote sensing datasets and the development of remote sensing theories and inversion techniques, remote sensing including microwave remote sensing will play a more important role in the studies and applications of the Earth systems.

microwave remote sensing, soil moisture, vegetation, snow water equivalent, land surface temperature

Citation: Shi J C, Du Y, Du J Y, et al. Progresses on microwave remote sensing of land surface parameters. Sci China Earth Sci, 2012, 55: 1052−1078, doi: 10.1007/ s11430-012-4444-x

Land surface parameters, such as snow, soil moisture, and vegetation, are important parameters of hydrology model, climate and land surface processes. It is difficult to monitor these parameters efficiently at large-scale, using traditional methods. In contrast to the traditional methods, remote sensing expands the limited information retrieved from conventional "point" measurements into the "surface" information and makes it possible to achieve quantitative analysis on the these parameters. Moreover, remote sensing provides concrete data basis and supports for quantitative analyses on land-atmosphere interactions and climate models.

Space-borne sensors are classified into three categories: visible, infra-red, and microwave sensors. Optical sensors are subjected to the influences of atmosphere and cloud

*Corresponding author (email: jshi@irsa.ac.cn)

whereas the microwave sensors have the all-weather, all-climate monitoring capacity. Besides the good penetration capacity, observations from microwave sensors are also very sensitive to water in variant forms, such as soil moisture, vegetation water content, and snow. With the launches of microwave sensors during the past years, microwave remote sensing has had the capacity of monitoring land surface at a global scale. Among these sensors, those designed for monitoring hydrology cycle and energy cycle are: (1) microwave radiometers with moderate or low spatial resolutions, including SMMR, SSM/I, TRMM, AMSR-E, and FY3/MWRI.These sensors have been used for the inversions of soil moisture and snow parameters; (2) microwave scatterometers with moderate or low spatial resolutions, such as ERS-1/2; (3) Space-borne SAR with high-spatial resolutions. These include TerraSAR-X,ALOS/PALSAR, RADARSAT-2, COSMO-SkyMed, and the scheduled HJ-1C SAR. (4) The scheduled L-band missions, such as the NASA SMAP mission.

Great efforts have been made in using the observations from these sensors. This paper will give a systematical introduction and review on the microwave modeling theory and inversion methods.

1 Theoretical modeling of microwave remote sensing

An accurate understanding and description of the microwave emission and scattering mechanisms of random rough surfaces, vegetation, and snow layer is the most important theoretical foundation, and provides the essential tools for the interpretation and explanation of satellite observations, simulation of satellite data, assimilation of satellite data, development of quantitative inversion algorithms of terrain parameters, as well as design of new sensors. We should thus strengthen the research on the theoretical modeling of microwave remote sensing. In the section we shall review the state-of-the-art of theoretical modeling of rough surface, snow, and vegetation for microwave remote sensing.

1.1 Modeling of scattering from random rough surfaces

The analysis of electromagnetic scattering from random rough surfaces has been one of the research hotspots in microwave remote sensing. The traditional models are the Kirchhoff Approximation (KA), which is applicable to surfaces with small curvatures or high frequency incidence, and the small perturbation method (SPM), which is applicable for slightly rough surfaces or extremely low frequencies. In order to bridge the gap between SPM and KA, several so-called unifying methods have been developed, including the phase perturbation technique (PPT) [1], the full wave approach (FWA) [2], the small slope approximation (SSA) [3], the integral equation method (IEM) [4], the operator expansion method (OEM) [5], and so on.

The ability to provide good predictions for scattering coefficients in certain applications and the convenience to use has made IEM a very popular model for the analysis of electromagnetic scattering from terrain surfaces. Its major assumptions are as follows: the removal of the spatial dependence of the local angle of incidence of the Fresnel reflection coefficient by replacing it with either the angle of incidence or the specular angle. For the cross-polarization, the reflection coefficient used to compute the Kirchhoff fields is approximated by one half of the difference between transverse parallel and vertical reflection coefficients; edge diffraction terms are excluded; and the complementary field coefficients are approximated by simplifying the surface Green's function and its gradient in the phase terms. These assumptions have compromised the model prediction accuracy, in particular for bistatic scattering, where notable discrepancy has been found between model results and measurements [6].

Concerns over the assumptions have prompted several modifications of IEM. Hsieh et al. [7] proposed the improved IEM model (I-IEM) where the absolute term in the exponent of the spectral representation of the Green's function was retained. As such, the complementary field coefficient F_{qp} contains both upward and downward travelling fields. Yet treatment of single scattering was kept identical to that of IEM, with modifications applied only to multiple scattering. Alvarez-Perez [8] proposed the so-called Integral Equation Model for Second-Order Multiple Scattering (IEM2M), where in addition to the retaining of the absolute term in the exponent of the spectral representation of the Green's function, the corresponding ±terms appearing in the gradient of Green's function was also kept. A decomposition of F_{qp} was made based on the Green's functions and their gradients in the subspaces above and below the rough surface. The two partial derivative components of the surface normal, obtained by the method of integration by parts, were also differentiated according to the Weyl spectral representation of the Green's functions in the subspaces above and below the rough surface. This treatment elicited different opinion from Fung et al. [9], for it was thought to cause oscillation when the medium below the surface was absorptive. Similar treatment was reported in the Advanced Integral Equation Model (AIEM) proposed by Chen et al. [10, 11], with a different treatment of the two partial derivative components of the surface normal, which was only based on the Weyl spectral representation of the Green's functions in the subspace above the rough surface. A transit function was used to modify the Fresnel reflection coefficient.

These modified models have demonstrated improved performance over IEM, in particular for bistatic scattering applications. However, there are still rooms for further improvement. First, the evaluation of the incoherent power of the complementary field is not sufficiently accurate. Second,

with the modification of the integration ranges due to the absolute term in the exponent, an error function should be resulted yet not reflected in the above models. Third, whether the two partial derivative components of the surface normal, when derived by the method of integration by parts, should be treated in the same way for media both above and below the surface, and if the answer is yes, then how to deal with the corresponding oscillation issue? Such analysis is still awaiting answers.

The Extended Advanced Integral Equation Model, (EAIEM) [12] can be regarded as an extension to both AIEM and IEM2M [13]. The extension contains two aspects: first in the evaluation of the complementary scattering coefficient for single scattering, it has made fewer, and less restrictive, assumptions; second, it has carried out a more rigorous analysis by the inclusion of the error function related terms for the cross- and complementary scattering coefficients, which can be regarded as correcting terms. The first aspect implies that the model for the complementary scattering coefficient is more accurate and more general, even when the effect of the error function related terms is neglected. The second aspect suggests that for the case where both the media above and below the rough surface are lossless, this correcting term vanishes for the cross-scattering coefficient, but not for the complementary scattering coefficient. Numerical results have demonstrated improved performance. An illustration is provided in Figure 1. However, there are cases where none of the above models can show good results, and further development of more advanced model is called for.

1.2 Modeling of scattering from snow

The modeling of scattering from snow needs to consider the impact of the microstructure of ice particles and their electromagnetic coupling, resulting in a rather complicated phase function. One typical theory is the Dense Media Radiative Transfer (DMRT) by Tsang et al. [13], where the coherent wave is treated using the Quasi-Crystalline Approximation (QCA), whereas the incoherent power by ladder approximation [14, 15]. The relative positions of ice particles are described by the Percus-Yevick pair distribution function [16]. This model can be used for active and passive microwave remote sensing with multiple-scattering effects. When combined with other methods, such as the Numerical Maxwell Model of Three-Dimensional Simulations (NMM3D), the theory was found to be in good agreement with measurement data [17].

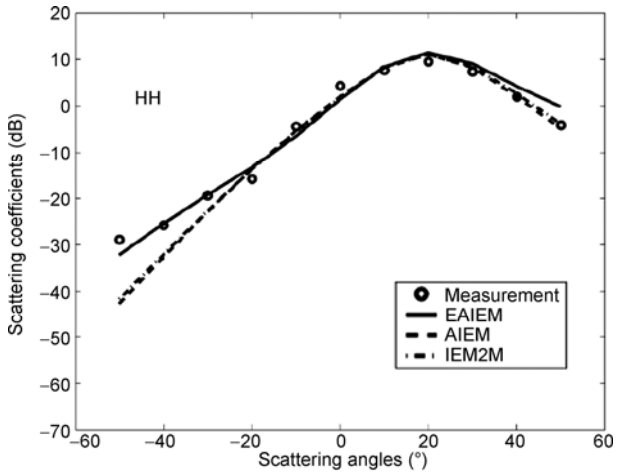

Figure 1 EAIEM Model shows precise theoretical predication for bistatic scattering coefficient.

Since the snow particles are treated as discrete ones in DMRT, the snow layer can be regarded as a discrete random medium. The alternative is to treat it as a continuous random medium, where the permittivity is a random variable described by its mean and spatial correlation function. Inclusion of the singularity of the dyadic Green's function leads to the strong fluctuation theory (SFT) [18].

Yet both upper and lower interfaces of the snow layer were assumed to be planar in DMRT with the effect of surface roughness in both surface scattering and surface-volume interaction ignored. The surfaces are rough by nature. To improve the modeling by including the effect of surface roughness, we proposed the DMRT-AIEM-MD microwave radiative model which is suitable for rough interfaces (Figure 2), and developed a parameterized multifrequency radiative model [19, 20], where propagation of the electromagnetic wave in the snow layer is described by DMRT, the contribution from the upper and lower surfaces is computed using AIEM, and the Matrix Doubling (MD) method for the analysis of multiple scattering within the layer [20]. Combining this model with the 0th order radiative transfer equation, we obtained a parameterized model. It has demonstrated an accuracy comparable with theoretical models and an efficient similar to that of the 0th order solution. In an analogous manner, we have developed a snow scattering theoretical model and parameterized model, which take into account vertical layers of the snow and multiscattering effect [21]. It has been demonstrated that the model agrees well with the measurement data and therefore can be used in an inversion algorithm for snow parameters as well as fast simulation of radar signals.

In addition, there are also other models such as the HUT model and MEMLS model that are simplified empirical snow radiative models. The HUT [22] model is based on the solution to scalar radiative transfer equation, with its scattering phase function simplified to contain only the forward direction (i.e., one Dirac delta function), whereas the extinction coefficient as a function of the snow diameter is obtained empirically [23]. MEMLS model [24] is a multilayer radiative transfer model for snow, suitable for 5–100 GHz frequency range. It is based on an approximate solution to the RTE, including the total reflection, coherent and incoherent reflections from the interfaces, whereas the snow scattering coefficient as a function of snow density

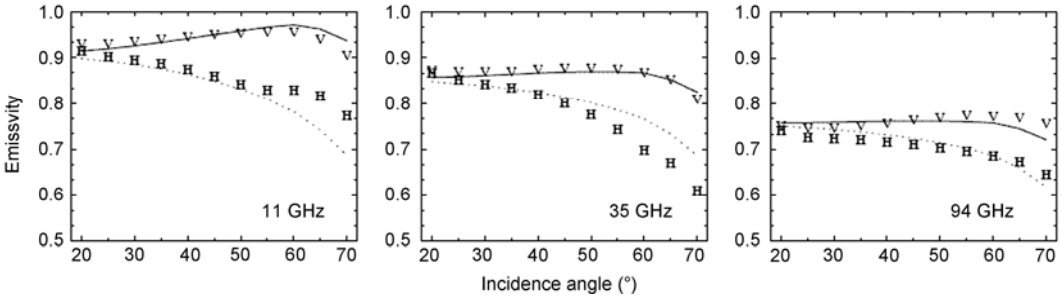

Figure 2 Comparison between snow's emissivity computed by DMRT-AIEM-MD model and measured.

and correlation length is obtained empirically [25], and the absorption coefficient, the effective dielectric constant and the reflection coefficients at interfaces are obtained through physical models and measured ice dielectric constant.

As the latest development in snow scattering models, Ding et al. proposed one model based on bicontinuous random microstructure with discrete permittivities [26], where the microstructure was simulated using the level-cut realization of Gaussian random field by Berk, which showed a great degree of similarity between simulated medium and realistic microstructure of snow [27]. The DDA was then used to calculate the scattered field, and the coherent and incoherent terms were separated after many realizations, where the incoherent wave was used for the computation of the phase function and scattering coefficient needed by RTE. This procedure gave a simulation of coupled active-passive microwave remote sensing. Because the snow geometrical structure was irregular in the Bicontinuous model, which was also similar to real structure to a large degree, the cross-polarized signal due to the irregular structure was accounted for and its prediction was thus improved.

1.3 Modeling of scattering from vegetation canopies

To model the scattering from vegetation canopies requires a good understanding of the involved complex electromagnetic interactions. Many models have been proposed in the literature. In the early models, a vegetation canopy was usually described as a continuous random medium with varying dielectric constant, and its scattering coefficient was obtained in terms of the variation and correlation function of the random dielectric constant. The calculation was relatively simple, yet the lack of direct correspondence between the parameters of the models and the physical parameters of vegetation canopies limit their usefulness.

The discrete random media models based on the physical parameters of the vegetation canopy have been proposed in the literature, where the canopy is treated as composed of discrete scatterers, whose scattering features are obtained through the averaging over the distribution of size, orientation, and dielectric constant of the scatterers. Typical models include the distorted born approximation (DBA) for single layer canopy by Lang et al. [28], and the Michigan Microwave Canopy Scattering Model (MIMICS) based on the Radiative Transfer Equation (RTE) by Ulaby et al. [29] In MIMICS, the vegetation layer consists of canopy, trunk and ground layers. The final outcome is the first order solution of the RTE. It has the following advantages: 1) in the analysis of ground scattering and the interaction between the vegetation and the ground, the effect of surface roughness has been included; 2) multiplicity of size and orientation of branches has been considered; 3) it is a fully polarized model. Karam et al. [30] proposed some refinement to the model, where second-order scattering within the vegetation layer was considered under the framework of RTE. The interference effect has been ignored in the above models. Sun and Ranson [31] proposed a three-dimensional radar backscatter model of forest canopies, where the effect of three-dimensional forest structure was considered. Ni et al. [32] further incorporated the matrix-doubling method into the model, which showed improved performance for cross-polarization.

Given the shortcomings of the incoherent models as listed above, the coherent model is increasingly taking a leading role. In general, the coherence of a vegetation canopy that needs to be considered in a coherent scattering model contains two parts: one is due to the constituents within a single plant, and the other due to inter-plant interaction. In a model that does not consider near field, the coherence is determined mainly by the relative positions of the scatterers. Each constituent is usually modeled using a canonical geometric form; for instance, for a single soybean canopy, the stem or a branch can be approximated by a dielectric cylinder of finite length, and a leaf by a thin dielectric disk. It has certain orientation distribution. The accuracy of a coherent vegetation canopy scattering model depends on several factors: 1) the accuracy of the analysis of scattering from the constituents, that is, from dielectric cylinders of finite length and from thin dielectric cylinders; 2) the accuracy of the analysis of scattering from random rough surfaces; 3) the degree of fidelity of representing the realistic scene; 4) the degree of importance of near field couplings among constituents; and 5) the accuracy of representing ground truth, such as the orientation distribution of a leaf.

As a dielectric cylinder of finite length is usually used to

approximate the constituent of many types of vegetation, it is important to accurately calculate its electromagnetic scattering. Different approximate methods are normally called for in the calculation depending on the shape, size of the cylinder and the wavelength. When the dimension of the cylinder is much smaller than the wavelength, the Rayleigh Approximation [28], Rayleigh-Gans Approximation, or Generalized Rayleigh-Gans Approximation (GRGA) can be used. GRGA is applicable to the case where the dimension of the cylinder is comparable to the wavelength, yet it is required that at least one dimension is much smaller than the wavelength. Stiles and Sarabandi [33] proposed a more general solution for dielectric cylinders of arbitrary cross section, yet the size of the cross section was required to be much less than the wavelength. When the length is much larger than the diameter of the cross section, the method of Infinite Cylinder Approximation (ICA) [34] can be used, where the internal field is approximated by that of infinite length. The GRGA and ICA methods have been widely used in the study of vegetation scattering. Yet caution must be made of their respective restrictions and the fact that the reciprocity theorem is satisfied by none of them.

For more general cases, Waterman [35] proposed a semi-analytical method called Tmatrix approach, which is based on the extended boundary condition method (EBCM). It has become one of the most widely used tools for rigorous solution of volume electromagnetic scattering based on Maxwell's equations, and has been applied to particles of various shapes, such as spheroids, finite cylinders, Chebyshev particles, cubes, and clusters of spheres [36–39]. In applying extended boundary condition to calculate the T matrix that relates the exciting field and scattered field, one assumes that the exciting field is inside the inscribing sphere and the scattered field outside the circumscribing sphere, respectively. However, for particles with extreme geometries such as very large aspect ratios, regular EBCM is found to suffer from convergence problems [40]. Physically, this ill-conditioning procedure is due to the fact that for cases of extreme geometries, the exciting fields will not accurately represent surface currents. Nor will the scattered fields.

For spheroids with a large aspect ratio, one approach for overcoming the problem of numerical instability in computing the T matrix is the so-called iterative extended boundary condition method (IEBCM) [41]. Its main feature is the representation of the internal field by several subregion spherical function expansions centered along the major axis of the prolate spheroid. The contiguous subregional expansions are related by matching in the overlapping zones. The point-matching method (PMM) can be used to determine the set of unknown expanded coefficients of internal field. In some spheroidal cases, the use of IEBCM instead of the regular EBCM is reported to allow more than quadruple the maximum convergent size parameter.

However, since this procedure approximates the highly lossy dielectric object with a perfectly conducting object of the same shape as its initial solution, it is restricted by the conductivities of the dielectric particles and the maximum convergent size parameter of EBCM for such perfectly conducting object. Moreover, as pointed out by Kahnert [42], PMM is less flexible for different particle shapes because, the more the particle's geometry departs from sphericity, the more unsuitable the expansions of the fields in spherical vector wave functions. Thus, elongated particles require the use of specially adapted PMM implementations with a longer computation time and higher computer-code complexity. Another similar technique is the general multipole technique (GMT) [43], which represents electromagnetic field vectors by multiple spherical expansions about several expansion origins, which are located at appropriate positions in the interior region. Although the GMT has been successfully used for particles with smooth surfaces, such as hemispherically or spherically capped cylinders, there are issues when it is used in the scattering computations of finite cylinders with flat ends reported. Recently, null field method with discrete sources (NF-DS) was proposed to deal with the instability of conventional EBCM [44]. Its numerical stability is achieved at the expense of considerable increase in computer complexity, and the resolution of this method can be affected by the localization of the sources.

For a cylinder with a large aspect ratio, the conventional EBCM suffers from divergence issue in the computation of the T-matrix, which is reflected in the instability of the solution. To this end, the so-called extended T-matrix method has shown to offer a good solution [45, 46].

The analysis of electromagnetic scattering from thin dielectric disk is mainly through the GRGA. Yet in this method the disk dimension is required to be much larger than the wavelength. Yet at L or C band, the representative dimension of the leaves of many types of vegetation is comparable to the wavelength (the resonant region), which brings forth a large degree of uncertainty in the suitability of the GRGA. Koh and Sarabandi [47] proposed a method that can be used over a wide range of disk dimensions in the calculating of the forward scattering amplitude function. Yet in this method, a key integral contains the product of two Bessel functions with distinct arguments, which may cause numerical instability for bistatic scattering. There is the need for further study in the analysis of electromagnetic scattering from dielectric disks.

As vegetation is treated as a discrete random medium, the electromagnetic coupling among main stalks, branches, and leaves may contribute to the overall scattering for the vegetation canopy. Its importance depends on, among other things, the type of vegetation and the wavelength. In the analysis of scattering from soybean canopy, Chiu and Sarabandi [48] proposed a simplified second order near field scattering to approximate electromagnetic coupling. They concluded that such near field is important at C band but not at L band. Yet a detailed analysis would reveal that the se-

cond order near field scattering has limited contribution to the overall scattered field even at C band. To be specific, at C band, although such near field scattering is significant for fully grown soybeans, for not fully grown soybeans, the same data show that the contribution from rough surface is about 10 dB higher for the horizontally-polarized backscatter up to 50°. Similar observations apply to the vertical polarization as well. Moreover, when computing scattering from the underneath rough surface, the roughness parameters used corresponded to a rather smooth surface, with the rms height and correlation length much smaller than the ground truth used in ref. [49], which seems to agree well with that in refs. [50, 51]. This suggests that the backscatter from the rough surface might be much stronger than that of ref. [49] had the common ground truth been used. In other words, the second order near field scattering is insignificant for not fully grown soybeans even at C band. On the contrary, the contribution from the underneath rough surface is higher, and may play a leading role in the overall scattered field in many cases.

The relative positions of vegetation plants may have a non-negligible effect on the overall scattering. The conventional branch model used hole correction, an first order statistical model, to describe the inter-plant topology. In ref. [52], the more complicated Percus-Yevick pair distribution function, originated from a statistical description of gas molecules distribution, was adopted to describe the inter plant distribution. In typical agricultural practice certain plants such as corn seem to form semi-regular rows and columns, or spatial semi-periodicity. Such semi-periodicity may be treated in a way similar to antenna array theory, with the modification that in setting up a two dimensional ground with periodically regular grids, one plant occupies a grid yet at random position within the grid. The random deviation of the plant from the center of the grid is assumed to follow a Gaussian distribution. Another important feature of a vegetation canopy is its anisotropicity at microwave frequencies, where the attenuation and change of propagation speed of the electromagnetic wave depends on polarization. The extinction coefficient and albedo for the horizontal polarization are different from that of the vertical polarization [53, 54]. Therefore a study of the anisotropicity is of theoretical and practical value.

The theoretical models are the foundations of microwave sensing and inversion of terrain parameters. In the following we shall provide a detailed survey of the inversion algorithms of major terrain parameters in microwave remote sensing. Specifically, we shall elaborate on inversion algorithms in passive as well as active remote sensing based on the distinct observation characteristics of microwave sensors.

2 Microwave remote sensing of snow

Seasonal snow is one of key parameters in water-energy balance prediction with the change of global system. It also influences the regional climate and hydrology, and acts as water resource for the mid-latitude areas. Therefore, it is very important to monitor snow cover's temporal and spatial variation.

2.1 Passive microwave remote sensing snow water equivalence retrieval

The microwave radiation from snow cover mainly includes two sections: one is the radiation form the snow itself, and the other is from the underlying surface. Snow's radiation changes with the volume of snow cover (snow depth), the structure of snow and the content of liquid water [55]. Both theory and experiments demonstrate that the brightness temperature decreases with the increasing snow depth [56]. In addition, snow grain size and liquid water content also strongly influence the brightness temperature of snow cover.

In low-frequency scope, the emission from dry snow cover is affected mainly by the properties of the underlying surface. On the other hand, the high-frequency emission is sensitive to the snow water equivalence and snow grain size, due to the scattering of the snow particles. [57, 58]. When snow starts melting, the emission from snow is enhanced obviously. That is because of the different dielectric constants of ice and water, while the main signals come from the snow surface [59]. Dry snow is strong scatter in high-frequency, but it absorbs little. Thus the scatter plays the dominate role in the extinction of snow in the high-frequency [60], which significantly decreases the direct radiation. So we can use this property to discover the existence of snow cover and retrieve the snow depth.

The study of monitoring snow using passive microwave remote sensing has been held for a long time in North America and Europe, and many researches about the physically based snow passive microwave remote sensing and algorithms have been taken, including theoretical models [20, 61, 62], ground-based measurements [63, 64], airborne experiments [65–67] and spaceborne experiments [68–73].

Since the 1990s, scientists in China combined the Chinese meteorological stations snow depth data with brightness temperature from SSM/I and AMSR-E, and developed several retrieval algorithms suited for Chinese area [74–76]. The main snow depth retrieval algorithms include semi-emprical, iterative and neural network algorithms and data assimilation methods. The signal received by the radiometer contains the emission from the atmosphere, snow pack, underlying surface, and the influences from vegetation. Due to these complex effects, it is difficult to develop some effective physically-based algorithms. The main algorithms to retrieve snow water equivalence are as follows.

2.1.1 Static snow water equivalence retrieval algorithm

Static snow water equivalence retrieval algorithm is one of most widely used algorithms over the world. These algorithms assume a linear relationship between the snow depth (or snow water equivalence) and the brightness temperature gradient. Researchers developed the empirical and semi-empirical methods to estimate snow depth and snow water equivalence. Based on the different data used during the algorithm development, researchers establish different linear empirical parameters a and b, where ΔTB is the brightness temperature difference of different frequencies and polarizations, which usually used the frequency 19 and 37 GHz at vertical or horizontal polarizations.

The accuracy of estimating the snow depth (SWE) is greatly complicated due to the presence of vegetation under which the radiation from the snowpack is weakened, while the signal received is increased because of the emission from the canopy. In order to improve the accurate estimation, Foster et al. [77] and Chang et al. [71] employed forest fraction cover to correct the algorithm under forest covered area. Foster algorithm [77] offered an improved method for the forest-cover area, and reduced the error from 50% to 15% in the SWE retrieval of North America. It ignored the difference at different areas, such as forest physical temperature, the type of forest, the density of the canopy, supposing the forest has the same contribution both in 18 and 37 GHz horizontal polarization brightness temperature. However, some problems still exist that when the canopy is thick, the microwave cannot penetrate it and the forest plays the dominate part of the radiation feature. Therefore, the signal from the snowpack under the canopy is less accordingly the error increases. Based on this feature, Forster et al. [77] employed two temporal dynamic parameters to represent effect of the forest cover percentage and snow grain size respectively, emphasizing the importance of prior knowledge such as snow classes and land-cover-type databases. Thus he established a new SWE retrieval algorithm. In addition, Derksen et al. [78] broadened the SWE retrieval in the boreal forest/tundra region in northern Canada.

Apart from the frequencies of 19 and 37 GHz, brightness temperature of other frequencies and land surface parameters are also employed in the static SWE algorithms. Because the microwave in 10.7 GHz can penetrate deeper snow than that in 18.7 GHz, Derksen [79] use the ground data from 2004 to 2007 to regress the relationship between the brightness temperature difference in different frequencies and SWE in the study of deep snow beneath the boreal forest of northern Canada. This study indicated that the deep snow with an obvious deep hoar layer also scattered and brightness temperature decreased with the increasing snow depth. In addition, to improve the poor retrieval results in Canadian tundra area, Derksen et al. [80] used the winter data from 2002 to 2006 to establish a new method only depended on the brightness temperature of 37 GHz in a vertical polarization.

In the study of retrieval algorithm in Chinese area, Cao et al. [81, 82] classified the southwestern China into five topographic units (plateau, higher mountain, lower mountain, hill, basin), then used optical snow data to validate the snow depth derived from SSMR data. Che and Li [83] improved snow depth algorithms with the Chinese weather station data. Sun et al. [84] and Chang [85] employed snow cover and MODIS IGBP land cover, referring the linear spectral unmixing method, using the Chinese meteorological station observed snow depth and AMSR-E brightness temperature data, to establish a snow depth empirical retrieval algorithm. On the study of their work, Wang [86] replaced MODIS IGBP land cover with the Chinese land.

2.1.2 Dynamic algorithm

Kelly et al. [87] developed a dynamic algorithm to estimate snow depth. The process of snow grain size and snow density is described with semi-empirical model changing with time. According to the relationship between the brightness temperature simulated by Dense Media Radiative Transfer Model (DMRT) and the snow depth, setting the snow temperature can return a quadratic polynomial regression equation. When the snow depth ranges from 50 to 100 cm, there is saturation points in 37 GHz, so Kelly set up the threshold to make sure the retrieval results is within the scope of the DMRT. The validation from global WTO-GTS station of 1992–1995 and 2000–2001 indicated its limited revision to Chang algorithm. Although the error is nearer to zero, its effect is no more significant than Foster algorithm [77].

Jobsberger and Mognard [88] developed the TGI (temperature gradient index) dynamic algorithm to interpret the temporal and spatial variation of the snow inner properties, especially the variation of snow grain size. Through the ground-based measurements in the Great Plains in the United States they found that the brightness temperature was still increasing after the snow depth reached the maximum and became decreased, which was contradict to principles of static algorithm. They thought it may be caused by the variation of the snow grain diameter. In certain stations, there is a linear relationship between SG and TGI, so the snow depth is easily derived. Although the TGI algorithm described the physical process in the snow variation, several problems remained: 1) this method is only adapted for the snowpack in Alaska, Siberia, and Canada and is valid only if Tground is below Tair. 2) The algorithm depends on differential equation as a function of time; therefore, when applied in daily retrieval, smoothing of time and Tair is required. 3) If the change in brightness temperature dSG/dt is the denominator, snow depth become abnormal when the dSG/dt is not significant. 4) This algorithm poorly predicts when the melting begins or when earlier snowfall melts after hitting the ground. 5) Due to the different snow variation processes in each year, the coefficient α is unstable with the annual change.

Based on the snow grain variation feature in the snow-

season, Grippa combined these static and dynamic algorithms discussed above to estimate the SWE [89]. This method predicts monthly snow depth relatively more accurate, but cannot be used in some areas such as boreal forest.

2.1.3 Iteration algorithm

One of well-developed iteration algorithms is The Helsinki University of Technology (HUT) model [73]. HUT as a forward iteration model is semi-empirical, given the influences from forest cover and atmosphere. Its basic hypothesis is that the radiation from snow is forward concentrated, accounting for 0.96. The snow is depicted as a single homogeneous layer. Snow extinction coefficient, forest canopy extinction, soil surface roughness, and the atmosphere effects are expressed by a semi-empirical equation. Roy et al. [90] used extinction equation for large particles, revising the algorithm on the basis of Rayleigh scatter. Pullianinen employed a least-squares method with constraint conditions with the HUT model to yield the SWE [73]. The brightness temperature derived from HUT model is in accord with the data observed by the SSM/I sensor. Hence the accuracy of HUT model is better than that of traditional static algorithms. The RMSE in regional SWE retrieval for dry snow is about 30 mm. However, this algorithm has a disadvantage that some atmosphere and canopy parameters as well as the soil surface roughness are yielded through the semi-empirical, and thus these parameters have a great regional difference. As a result, the relative error varies from year to year, and the minimal RMSE is around 20 mm.

2.1.4 Physically-based algorithm

Jiang et al. [20] adopted the matrix doubling approach to calculate the snowpack vector radiative transfer equation. This model uses DMRT model on the basis of Mie scatter to interpret the extinction and emission in the snow layer, and then uses AIEM to establish the boundary conditions of surface emission and vector radiation transfer model. Owing to the complex equation of Matrix Doubling approach in considering the multiple scattering, the answer to it cannot be used in retrieval. Hence, Jiang et al. [91] analyze the multiple scattering-considered model and compare it to the zeroth-order model, developing a parameterized model that includes multiple scattering. This model is adapted for the condition that the optical thickness τ below 2. Based on the parameterized model, Jiang et al. [91] developed the model-based SWE retrieval algorithm.

On the basis of establishing an emission simulation database containing more snow parameters as possible, Jiang et al. [91] used the thought discussed above to obtain the snowpack emission (A) and attenuation properties (B), and then according to the simulated data, found the good regression relationship between these two parameters, which means the SWE can be calculated through it.

$$swe \approx \exp[a + b \cdot A + c \cdot A^2 + d \cdot \log(B)], \quad (1)$$

where a, b, c, d is the regression coefficient established by the data base. Note that A, B is only affected by the snow properties. Suppose the snow particle is sphere-shaped and random distribution, A, B is free with the polarization. Therefore, A and B can be deducted by two given frequencies and polarizations values:

$$B = \frac{E_v^t(f_1) - E_h^t(f_1)}{E_v^t(f_2) - E_h^t(f_2)}, \quad (2)$$

$$A = E_p^t(f_1) - B \cdot E_p^t(f_1). \quad (3)$$

This algorithm uses simulated data to validate. Figure 3 is the comparison between SWE derived from simulated data and the input (as the true value). The RMSE is 32.8 mm, indicating that the model can be used directly to retrieve the SWE.

This algorithm assumed that the surface temperature and snow temperature are known. Firstly, use the relationship between different frequencies and polarizations to remove the effects caused by the surface in the whole observed signals. Then extract the signals from the snowpack to retrieve the SWE. Jiang et al. [91] used the radiation stimulated database and airborne data from the Cold Land Processes Field Experiment (CLPX, 2003) in Colorado to test this method, and the accuracy in SWE estimation reaches 30 mm. Comparing this results and that from the basic algorithm used by AMSR-E to ground measurements, they found that both methods overestimated the SWE. However, the new physically-based statistic algorithm is more accurate than the AMSR-E one. But this algorithm can only perform in vegetated sparse area. It needs to be further work in dense vegetated regions.

2.1.5 Neural network algorithms

At first scientists use the Backus-Gilbert techniques to solve remote sensing problems. They use single-scattering approximation to conveniently describe the linear relationship between scatter measurements and the medium parameters. But in the problems about microwave remote sensing, espe-

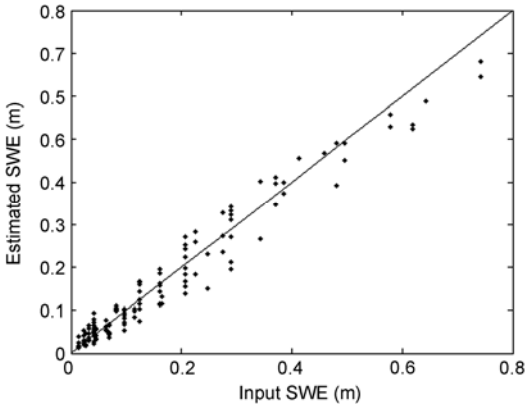

Figure 3 Comparison between snow water equivalence data simulated and retrieved.

cially the dry snow, multiple scattering play an important role, and there is a nonlinear relationships between measurements and medium. At present, the neural network technique is used in multiple-parameter retrieval. Davis et al. [92] trained the snow signal simulated by DMRT model including multiple scattering and extracted snow parameters, where they use five measurements to yield four parameters (mean snow grain size, snow density, snow temperature and snow depth). Because of the presence of problems, this technique has some difficulties with a wide application, especially the limits of the trained data.

2.1.6 Data Assimilation methods

Liston et al. [93] and Rodell et al. [94] used the earliest data assimilation methods, which update snow depth with a direct-insertion, that is, replacing the model simulation with the direct observations, directly substituting the simulated results in a coupled land-atmosphere simulation, so as to improve the simulation of SWE. In some conditions it can improve the simulation, but sometimes the streamflow does not predict correctly [95]. Sun et al. [96] applied the extended Kalman filter to assimilation based on the watershed land surface model, which remained on the pre-research of the snow assimilation methods [97].

Andreadis and Lettenmaier [98] applied an ensemble Kalman filter to couple the remote sensing snow monitoring to the Variable Infiltration Capacity (VIC) model. They utilized the MODIS snow pack product from 1999 to 2003 to update the SWE simulated by the VIC, retrieving the SWE and snow cover resort to a simple snow melting model. The results indicate that mean absolute differences in snow coverage of 0.106 and 0.128 for assimilating MODIS snowpacks or not, respectively. Andreadis and Lettenmaier assimilated the AMSR-E SWE product, but because it does not work in the deep snow. Thus, the accuracy will decrease if applying the remotely sensed SWE when the snow is deep.

Durand and Margulis [99] assimilate the SSM/I and AMSR-E brightness temperature and broadband albedo to the Simple Snow-Atmosphere-Soil (SAST) model put which is inside the Simplified Simple Biosphere, testing the feasibility in SWE estimation and improving the estimation accuracy. They also found, among the whole microwave band of SSM/I and AMESR-E, the 10.65 GHz band can provide the most of SWE information.

Based on HUT model, Pulliainen [100] applied the assimilation microwave brightness temperature observing approach and the Bayesian technique, adding different weights to each snow depth from the satellite observation and ground-based measurements and improving the retrieval accuracy with the assimilation technique. At present, this approach is used in North America snow depth and SWE retrieval algorithms, established by Finland Meteorological Institute in Europe. In addition, Che [101] combined the MEMLS model with the snow cover module in CLM to study the indirect snow parameter assimilation. Because of the difference of the direct assimilation data and satellite-based retrieval data, the ultimate results will be affected. The indirect assimilation with the resort to radiation transfer model and snow cover physical process model can assimilate the brightness temperature observed by the satellite. Thus it can efficiently reduce the error brought by the satellite observation during the snow physical process.

In summary, currently the common passive microwave snow depth (SWE) retrieval algorithm is the semi-empirical linear algorithm. This sort of algorithm can estimate accurate snow depth in specific areas, while there are still uncertain factors when applied in the global application. And other techniques such as neural networks, iteration, Bayesian retrieval algorithms are difficult to be carried out in the whole world. We suggest to establish a physically-based theoretical retrieve model, which could estimate snow depth and snow water equivalence. And it will help us to understand snow microwave emission character in the aspect of physical scheme.

2.2 Snow parameters retrieval by active microwave remote sensing

Compared with passive microwave sensors, unique information related to polarization, intensity and phase signatures are provided within the active microwave sensors, especially the Synthetic Aperture Radar (SAR). By using these additional information, the active microwave remote sensing has advantages in high resolution snow mapping and snow parameters retrieval.

2.2.1 Snow mapping with SAR

Visible and near-infrared sensors have been used intensively for snow mapping, but they are limited by weather condition and cloud, and thus it is very essential to study the method of snow mapping by active microwave sensors. Three different methods are usually used for snow mapping by SAR, as described below.

(1) Snow mapping with single-polarization multi-temporal data. Only one intensity measurement per pixel is available with single-polarization data, and thus we only rely on the radiometric property to distinguish snow covered area from other targets. Because of the unique dieletric property of wet snow at microwave band, the backscattering coefficient of wet snow area is usually lower than other targets such as bare soil and dry snow area. By using this property, multi-temporal data acquired with snow-free (or dry snow) and wet snow condition can be used for wet snow mapping [102]. The imaging geometry of multi-temporal data is similar, and thus this reduced the terrain effect on the algorithm. For wet snow mapping in forest regions, the first step is to compensate forest canopy effect on observed backscattering coefficient. This is done by a semi-empirical forest backscattering model and forest stem volume infor-

mation [97]. Then the fraction of wet snow covered area is calculated with the estimated ground surface backscattering coefficient and two reference images: one with fully wet snow cover and the other with snow-free condition [103, 104].

(2) Snow mapping with multi-polarization and multi-frequency observations. Shi and Dozier [105] evaluated the characteristics of the backscattering coefficient, polarization, and frequency ratio of the targets in the study site near the Mammoth Mountain. They developed two types of supervised classifiers based on classification tree technique. The first type of the classifier was developed by using intensity measurements, polarization properties, and frequency ratios. It can map dry snow and discriminate dry from wet snow, but it requires topographic information for radiometric terrain correction and to reduce effects of local incidence angle. It is about 79% as accurate as a TM binary classification, but it suffers some shortcomings; for example, it underestimates the total snow cover in regions of mixed pixels, especially forested regions. Its performance on the two data-takes where the snow was dry showed that only a few pixels were misclassified as wet snow. The second type of classifier was developed based on polarization properties and backscattering ratios between different frequencies. Since these measurements can be obtained correctly without radiometric terrain calibration, the classifier does not require topographic information and can be used to map wet snow. Shi et al. [106] also developed a method with multi-polarization C-band airborne SAR to map wet snow and glacier ice without a DEM, using only measurements of the polarization properties. Its accuracy is 77% when compared with TM binary classification.

(3) Snow mapping with repeat-pass Interferometric technique. In the study of using SIR-C/X-SAR data to map snow cover [105], it was found that wet snow cover had very similar backscattering intensity and polarization characteristics to smooth bare surface at C-band and X-band. In a large drainage basin or at the regional scale, where many different targets are within a scene, those intensity based techniques might not be reliable. For similar reasons, change detection measurement might be also unreliable since the similar change in backscattering could be caused by different natural environment changes. Thus, other techniques should be developed for large-scale snow mapping.

Repeat-pass data provides additional measurement other than the intensity, the coherence measurement between two repeat-passes is a useful measurement in addition to backscattering intensities in each scene and their changes between two passes, and makes it possible to develop an algorithm for mapping both dry and wet snow covers over large area. Strozzi et al. [107] demonstrated that coherence measurements could provide the separation between wet snow cover and bare ground. The low coherence observed over wet snow cover is caused mainly by the rapid change in scattering properties and geometry as a result of wet snow metamorphism due to the movement of free liquid water content, ice grain growth, displacements of adjacent scatterers, and formation of density heterogeneities (layering, ice-lenses, etc.), which all result in a significant decorrelation. On the other hand, the high coherence is regularly observed over no-forested snow free areas. For forested areas, it can be easily separated with wet snow cover due to their significant difference in backscattering intensity even if its coherence is generally low. These are the physical basis for wet snow mapping. For using C-band measurements, however, it requires the short temporal scale (a few days) between the two repeat-pass measurements in order to avoid the significant temporal decorrelation in other surface targets such as bare or short vegetation surfaces.

Shi et al. [108] evaluated the L-band coherence measurements between two repeat-pass SIR-C image data from its first mission in April (with snow) and second mission in October (without snow), 1994. They showed that the coherence measurements between one snow covered scene and one without snow provide a very good separation between snow cover and bare surface as well as short vegetation. A pixel-based decision tree classifier was developed based on analysis on coherence and intensity. The coherence and intensity information were both used in the classification tree. Comparison showed that 86% accuracy was achieved for snow cover area under consideration of the TM classification map as the ground truth.

Venkataraman et al. [109] used the full polarization ALOS PALSAR data for snow mapping. This method was based on H-A-α polarization decomposition technique and the feature that the "Polarization Fraction" index is higher in snow covered areas than other areas. The third eigen value of H-A-α decomposition was also used for the mapping algorithm. Comparing with the results of H-A-α Wishart supervised classification and Yamaguchi decomposition Wishart supervised classification showed that this method can produce fairly good snow mapping result and does not need any topographic information [109]. Longepe et al. [110] also used the full polarization PALSAR data for snow mapping. The Support Vector Machine (SVM) technique combined with H-A-α decomposition, or Freeman decomposition or the three polarized backscattering intensity were used for mapping of snow-free area, wet snow area and "dry snow & frozen soil area". The result comparisons indicated that SVM technique combined with Freeman decomposition quantities produced the best result [110].

2.2.2 *Snow parameters retrieval with SAR*

(1) Snow wetness inversion. Shi and Dozier [111] developed an algorithm for snow wetness retrieval using C-band polarimetric SAR imagery. This algorithm is developed using a database, which covers the most possible wet snow physical properties including the wide ranges of snow wetness, density, particle size and surface roughness, simulated by the first-order scattering model with both sur-

face and volume scattering components. The major developments in this algorithm were: 1) a simplified surface backscattering model, that describes the relationships between the different polarization measurements for the conditions of most seasonal wet snow covers, to minimize the surface roughness effects with multi-polarization measurements; 2) the property of the volume scattering ratio in co-polarizations, which is only a function of snow permittivity and incidence angle to minimize the volume scattering albedo effects on estimation of snow wetness. This algorithm requires no information about the volume scattering albedo or the surface roughness parameter. With known local incidence angle, it involves only the calculation of snowpack permittivity, which can be directly related to snow wetness. This algorithm is applicable to the situations of incidence angle from 25° to 70°, and the snow surface roughness — rms height <0.7 cm and correlation length <25 cm. The comparison between ground measured snow wetness and snow wetness derived from SIR-C and AIRSAR using this algorithm showed that the algorithm performed well on both local and regional scales and provided a quantitative estimate of spatial distribution of snow wetness at the top snow layer.

(2) Snow water equivalence estimation from SAR. Various ground experiments showed different relationships between radar backscattering coefficient and Snow Water Equivalence (SWE). For example, Ulaby and Stiles [112] showed that backscattering at 8.2 and 17.0 GHz had a positive relation with SWE. Similarly, a positive relationship was also observed by an experiment over a smooth subsurface at 5.3 and 9.5 GHz [113]. On the other hand, negative relationships have been observed at similar frequencies, 5.3 and 9.6 GHz [107]. In addition, Rott and Matzler [114] observed no significant difference between snow-free and dry snow covered regions at 10.4 GHz. Each field experiment represented particular snow and ground conditions. The existence of both positive and negative relationships between radar backscattering and snow water equivalence indicates that this relationship is quite complex. Radar backscattering coefficient measurements over seasonal snow covered terrain can, generally, be expressed as a four component model:

$$\begin{aligned}\sigma_{pq}^{t}(f) &= \sigma_{pq}^{a}(f)+\sigma_{pq}^{v}(f)+\sigma_{pq}^{gv}(f)\\ &+T_pT_qL_pL_q\sigma_{pq}^{g}(f),\end{aligned} \tag{4}$$

σ_{pq}^{a} is the backscattering from snow surface, σ_{pq}^{v} is the volume backscattering from snow layer, σ_{pq}^{gv} represents the interaction term between snow volume and the snow-ground interface, and σ_{pq}^{g} is snow-ground interface backscattering. The subscripts p and q represent polarization status of the observed radar signals, T is the power transmittivity at the air-snow interface, L is the snow-pack attenuation factor. The SWE inversion algorithm can be developed based on accurate backscattering model and deep understanding of the scattering mechanisms. The classical algorithm is the algorithm developed by Shi and Dozier [115], which used multi-frequency (L, C, X band) and dual polarization (VV and HH) data for SWE inversion.

This algorithm uses L-band measurements to estimate snow density and the underground dielectric and roughness properties. The relationship between underground backscattering signals at C-band and X-band can be estimated with the dielectric and roughness properties estimated from L-band measurements. Then, using C-band and X-band measurements with the minimized effects of the underlying backscattering signals estimates snow depth and ice particle size. This algorithm requires all 3 SIR-C/X-SAR frequency measurements. The detail of this algorithm is as follows.

First, L-band measurements were used to estimate snow density and the underground dielectric and roughness properties. At microwave frequencies, the absorption coefficient (the imaginary part of the dielectric constant) of ice is small, and snow grains are also small compared to an incident L-band wavelength (24 cm). Thus, when the electromagnetic wave passes through the snowpack, versus directly striking the ground, the following differences occur: the incidence angle at the snow-ground interface is smaller, the incident wavelength at the snow-ground interface is shorter because the snow is dielectrically thicker than air, the reflectivity at snow-ground interface is reduced due to the lower dielectric contrast at the snow-ground interface than the air-ground, and the total energy incident on the snow-ground interface is reduced due to the power loss at the air-snow interface. Based on the above understanding of snow density effects on radar backscattering at L-band, Shi and Dozier [115] developed an algorithm to estimate snow density by characterizing the dependence of the surface backscattering on both the incidence angle and the wavelength. It was done by establishing a VV and HH polarization backscattering database using the IEM model [9] over a wide range of incidence angles, dielectric and roughness conditions, and incidence wave numbers, corresponding to a range of snow densities from 100 to 550 kg/m^3. Then, the relationship of HH and VV backscattering signatures with the wide range of surface dielectric and roughness conditions at each incidence angle and wave number was characterized by using regression analysis. In the algorithm, for a given L-band SAR measurements of VV and HH SAR data, we can estimate the snow dielectric constant. It does not require a priori knowledge of the dielectric and roughness properties of the soil under the snow. Furthermore, snow density can be estimated from Looyenga's semi-empirical dielectric formula. After the snow density, ground dielectric constant, and surface RMS height were estimated by L-band SAR measurements, through analyses of the simulated data, the techniques for estimating snow depth and ice particle

size using SIR-C C-band and X-SAR measurements were developed by Shi et al. [116]. The main idea in this algorithm is to develop a semi-empirical model to characterize the relationships between the ground surface backscattering components at C-band and X-band, and to parameterize the relationships between snowpack extinction properties at C-band and X-band. Finally, the SWE can be calculated by the estimated snow density and snow depth.

The technique described above for estimation of SWE requires five measurements: L-VV and L-HH to estimate snow density and ground dielectric and roughness properties, plus C-VV, C-HH, and X-VV to estimate snow depth and grain size. The sensitivity analysis indicated that the C-band SAR measurements were affected mainly by the ground surface properties. The parts of the signal that comes from a typical snowpack at C-band are about 30% and 15% for HH and VV polarization, respectively. The C-band measurements are expected mainly sensitive to soil surface condition below snow layer. Estimation of snow depth using C-band SAR measurements, therefore, requires an accurate technique to estimate the ground backscattering component. At X-band it about 60% of the signal comes from the snowpack itself. Thus, we expect that the measurement is much more sensitive to snowpack and that the requirement for estimation of the ground backscattering component is less severe for radar measurements at X-band or higher. The global SAR snow monitoring programs such as ESA CoReH2O and NASA SCLP both adopted high frequency polarimetric SAR (X and Ku band), and the corresponding research on the inversion algorithm has also been carried out. For example, Shi proposed an algorithm to estimate the volume backscattering from total observed backscattering by de-polarization index, and then the SWE was estimated by dual-frequency observations, which is an important possible solution [117, 118].

3 Soil moisture retrieval with microwave remote sensing

Soil moisture is one of the most important parameters on the land surface. Due to its significant influence on the global water cycle, energy balance and the climate variation, soil moisture monitoring on the local and global scale is an essential condition for the research of global water cycle rule, watershed hydrological model, and the monitoring of crop growth and drought. The main methods to retrieve surface soil moisture with microwave remote sensing are active microwave remote sensing methods based on Radar or scatterometer, passive retrieval methods based on radiometer, and the methods combining both active and passive microwave remote sensing. The active microwave can provide high spatial resolution, and is sensitive to surface roughness and vegetation construction, but with a complex data processing and low revisit rate. However, the passive microwave can provide high temporal resolution, and is sensitive to the soil moisture and with a simple data processing. But the spatial resolution is low. Therefore, more and more researchers consider combining them both and taking the advantages of each in the retrieval of surface soil moisture.

3.1 Passive microwave soil moisture retrieval

With a highly temporal frequency, passive microwave remote sensing provides measurements for daily regional and global soil moisture retrieval. There already have been several space-borne microwave radiometers, including SSMR, SSM/I, FY-3, WindSat, AMSR-E, and SMOS etc. SSMR, SSM/I, FY-3, WindSat, and AMSR-E are multi-frequency configured, whose lowest frequency band is not lower than C-band. Since radiometer with a lower frequency band is more sensitive to the soil moisture, soil moisture retrieval mainly uses measurement of C-band, X-band or Ku-band as input data. However, as the signal's penetrability of vegetation layer in these frequencies is limited, soil moisture retrieval with these bands is only applied to area of the bare soil and low vegetation. For obtaining the precise soil moisture of land covered by vegetation, the lower frequency instrument is required. At present, researchers are focusing on the soil moisture retrieval algorithm specific to the instrument of L-band. SMOS is designed by European Space Agency (ESA) for retrieving soil moisture and ocean salinity, launched in Nov. 2009. SMOS is the first radiometer receiving the earth's emission energy at L-band by the interferometry technique. SMOS has superiority at instrument configurations, which are multiple incidence angles and L-band frequency having good penetrability of vegetation layer and more sensitive to soil moisture. Compared to the AMSR-E, it is more reliable and more precise. The on-going NASA Soil Moisture Active and Passive (SMAP), mission will observe the earth using combined active and passive secsors at L-band. SMAP will provide more precise soil moisture information and enhance the spatial resolution.

Current soil moisture retrieval algorithm of AMSR-E is iterative method. By using ω-τ as forward model to calculate theoretical brightness temperature values, the soil moisture estimates are adjusted iteratively until the difference between the computed and observed brightness temperatures is minimized in a least squares sense. The retrieval algorithm of SMOS follows the AMSR-E's. However, research results show that there are some shortcomings in the algorithms of SMOS and AMSR-E.

Firstly, bare surface emission is described by the semi-empirical model Q/H model, and Q/H model has the assumption of the equal effect of the surface roughness on surface emissivity in both v- and h-polarizations [119, 120]. But, there is a big error between the surface roughness from

the field measurements and the surface roughness fitted by the Q/H model from the soil moisture measurements or dielectric constant. Recently, through researching on the theoretical surface emission model integral equation model (IEM) [19, 121], it indicates that for the two different polarizations, the effect of roughness on the effective reflectivity or emission differs in both magnitude and direction, which depends on the incidence angle, surface roughness and dielectric character. At big incidence angle such as AMSR-E, effective surface reflectivity in V-polarization is greater, but in H-polarization the effective reflectivity is smaller than Fresnel reflectivity at the same soil moisture. This effects the description of the relationship between V-polarization emission signal and H-polarization, especially on the amount of V/H polarization ratio, leading to the error of soil moisture estimated from the V- and H-polarization measurements. Shi et al. [121] developed a method for retrieving soil moisture using the V- and H-polarization measurements to minimize the effect of roughness.

Secondly, iterative method has some shortcomings [122]. Measurements of microwave radiometer depend on surface soil moisture, roughness, attenuation, and extinction of the vegetation layer, as well as temperature of soil surface and vegetation canopy. Through constructing cost function, adjusting model parameters, and minimizing the difference between the computation and measurements, iterative method retrieves the soil moisture. In the procedure of soil moisture inversion, other physical parameters such as surface roughness, attenuation, and single scattering albedo of the vegetation layer, temperature of soil and vegetation canopy, have effects in minimizing the difference between the value simulated and the value measured. So, iterative algorithm cannot be used to determine which variable changes the amount of satellite measurement in mechanism. Iterative method has the problem of multiple solutions. Through developing the retrieval theory based on the physical model, it is helpful to overcome the above shortcomings and improve the inversion accuracy. In addition, passive microwave soil moisture retrieval algorithm also includes neural network (NN) method [123–125].

3.2 Active microwave remote sensing of soil moisture

Radar backscattering coefficient is affected mainly by the surface characteristic, such as surface roughness, dielectric constant of soil, and property of vegetation layer. In order to perform soil moisture retrieval, we need to establish the relationship between the radar scattering coefficient and soil volumetric water content. For bare ground and sparse vegetation, the researchers have achieved remarkable success in the study of the algorithm of soil moisture retrieval. As for the case that vegetation effect cannot be neglected, the researchers have also made some progresses. We will briefly introduce the retrieval algorithm for the bare surface case and vegetated surface below. Because the inversion often belongs to the "ill-posed" problem, there must be uncertainty relationship between scattering coefficient and soil moisture. But the use of multi-polarization radar observations can reduce the uncertainty, and illustrate a more precise relationship between the two. For the case of bare ground and sparse vegetation surface, the researchers have developed a quantitative retrieval algorithm of soil moisture from dual-polarized L-band SAR image [126, 127], or from three polarization radar observation [128]. Based on simulated backscatter of bare surface of different surface roughness and soil moisture conditions by IEM model, Shi et al. [127] developed a semi-empirical bare surface backscattering model, establishing the relationship between L-band VV and HH polarization backscatter coefficient, dielectric constant and surface power spectrum of roughness, which is shown in eqs. (5) and (6). This model used simulation data of a theoretical model to overcome the dependence of the specific site data, with a certain degree of universality.

$$10\log_{10}\left[\frac{|\alpha_{pp}|^2}{\sigma^0_{pp}}\right]=\alpha_{pp}(\theta)+b_{pp}(\theta)\cdot 10\lg\left[\frac{1}{sr}\right], \tag{5}$$

$$10\log_{10}\left[\frac{|\alpha_{vv}|^2+|\alpha_{hh}|^2}{\sigma^0_{vv}+\sigma^0_{hh}}\right]=\alpha_{vh}(\theta)+ b_{vh}(\theta)\cdot 10\lg\left[\frac{|\alpha_{vv}||\alpha_{vv}|}{\sqrt{\sigma^0_{vv}\sigma^0_{hh}}}\right], \tag{6}$$

where α_{pp} is polarization amplitude, *sr* is roughness parameter, and σ^0_{pp} is backscatter coefficient.

The above model is established for the bare ground or sparse vegetation cover conditions. If we take the algorithm for inversion of soil moisture for vegetation cover surface, it will cause underestimation of the soil moisture content or overestimation of the surface roughness. To better understand the effect of vegetation layer on radar backscatter, the current study of soil moisture retrieval for vegetated surface is mainly the following:

(1) Inversion algorithm using Multi-polarization data [129]. In order to inverse soil moisture under low vegetation cover, the algorithm first assumed that the vegetation layer consists of randomly distributed dielectric discs, and then created a simulation database based on the radiative transfer model. According to the simulation database, the algorithm first divides the total scattering into two parts: one part is directly from the soil surface attenuated by the vegetation layer; the other part is the combination of vegetation scattering and vegetation-surface interactions. The surface scattering component can be accurately separated by this algorithm for the VV, HH, and VH polarization, with the root mean square error 0.12, 0.25, and 0.55 dB respectively. After the separation, the soil moisture and comprehensive correction factor of surface roughness and vegeta-

tion attenuation can be estimated. For the simulated data, the mean square error can be less than 4%.

(2) Inversion algorithm using combination of ancillary data and radar data. For correction of vegetation effects, based on empirical relationships, the optical data or synchronized measurement data (vegetation water content, leaf area index, etc.) are used to estimate vegetation scattering components and vegetation attenuation factor, through which the impact of vegetation on radar observations can be corrected and the soil moisture can be estimated [130, 131].

(3) Soil moisture change detection algorithm using repeat observations. Due to the complexity of the problem of scattering of surface under vegetation cover, using short-period repeated radar observations to estimate changes of soil moisture is the start point of the current study. If the surface roughness and vegetation are considered within a certain period of time, the difference of scattering coefficient between repeated radar observations could be attributed to changes in the surface dielectric constant. Therefore, repeated observations can provide information of the relative change of soil moisture, and thus improve the accuracy of soil moisture inversion.

The key to the realization of this method is how to correct the influence of vegetation. The researchers proposed different algorithms. For example, one can apply the Freeman's decomposition technique [132] or utilize optical auxiliary data to correct vegetation volume scattering [133], then use the ratio of two observations to estimate the relative changes in soil moisture.

3.3 Combined active and passive microwave remote sensing algorithms

The approaches used combined active and passive microwave remote sensing to retrieve soil moisture may be broken up into the following categories: (i) The forward model of active and passive are made respectively according to the relationship between remote sensing data and soil surface parameters, and then soil moisture and vegetation properties were estimated simultaneously. Lee et al. [134] used the 10.7 GHz Tropical Rainfall Measuring Mission (TRMM) microwave image (TMI) channel and 13.8 GHz precipitation radar(PR) observations to estimate the near surface soil moisture and vegetation properties. The adopted strategy was first to calibrate the emission/backscattering model parameters (using *in situ* observations of soil moisture and LAI) to adequately specify the integrated nature of vegetation canopy and soil properties. Subsequently, the calibrated models were used within an inverse solution to retrieve soil moisture and LAI by simultaneously minimizing the disagreement between simulated and satellite measured brightness temperature and backscatter coefficients. The technique was applied on TRMM radar/radiometer observations from three consecutive years and evaluated against in situ near-surface (5 cm) soil moisture measurements from Oklahoma Mesonet, showing a consistent performance. The active backscatter coefficients were simulated by Geometric Optics Model (GOM) and water-cloud model for vegetation correction. The ω-τ was used for brightness temperature simulated, the empirical model of Jackson was for vegetation and a constant was assigned to surface roughness. In the algorithm, the active measurements as an additional channel are combined to the passive channel. This was good for the iterative inversion but did not take full advantage of the high spatial resolution of active observations. The difference on the spatial scale between active and passive microwave data was not sufficiently explained. Additionally, the model requires many ancillary data, which limits its global application. The iterative algorithm cannot explain the relationship of the various parameters in the model. (ii) The surface roughness and vegetation parameters were estimated from active microwave measurements then used in the passive model to inverse soil moisture. O'Neill et al. [135] proposed a combined active and passive microwave soil moisture retrieval algorithm under vegetation cover. L-band radar was employed to calculate vegetation transmissivity and scattering using discrete vegetation scattering model. These parameters were then used in a soil moisture prediction algorithm based on the passive microwave data from L-band radiometer. The predicted soil moisture of two experiments matched to that measured was excellent, with RMSE of about 2.4%. However, in the algorithm, surface roughness correction was not explained and the in situ measurements of canopy geometry were required in estimation vegetation parameters using active microwave data. (iii) The active microwave data are combined with passive observations based on the mathematical methods to retrieve soil moisture. Njoku et al. [136] combined radiometer and radar measurements of the Passive and Active L-band and S-band airborne sensor (PALS) during the 1999 Southern Great Plains (SGP99) experiment to retrieve soil moisture using the change detection method. Assuming that the effects of vegetation and surface roughness are relatively invariant on the short time scales, the change of radiometer or radar observations is only due to the soil moisture variant. The approximate linear relationship between the radar measurements and soil moisture was also hypothesized. Soil moisture for two different conditions, "dry" and "wet", were first estimated using the H polarization of L-band. Then the estimated soil moisture under two conditions was used as "truth" with radar data to calibrate the slops and intercepts of radar liner equations. These coefficients were then used to derive soil moisture using radar data only. Soil moisture derived by this algorithm has good accuracy in the calibration period, and the temporal and spatial distributions show similarity to those from radiometer data. However, with temporal changes the accuracy of estimated soil moisture decreases due to the applicability of calibrated coefficients, vegetation changes, and other factors. Narayan et al. [137] applied the algorithm and hypothesis similar to Njoku to

estimate soil moisture combined active AIRSAR with PALS passive data acquired during SMEX02 campaign. The approach takes advantage of the approximately linear dependence of radar backscatter change on soil moisture change as vegetation unchanged. The ratio of radar backscatter coefficients change to soil moisture considered as an effect factor of vegetation and surface roughness. It was assumed that the change of soil moisture measured by radiometer at lower spatial resolution is equal to the average of all the radar observations within it. All the radar pixels within the radiometer pixel were given uniform vegetation and surface roughness characteristics. So the relationship of soil moisture change between active and passive was made. The soil moisture change in the radar pixel can be estimated if the change of radiometer pixel was known according to the relationship between them. Though the algorithm improves spatial resolution, the result is just the soil moisture change. In the case of the SMEX02 experiments, each radiometer footprint lies completely within an agricultural field with fairly uniform vegetation characteristics. In fact, the revisit time of current space-borne active microwave sensors cannot meet the requirements and it is difficult to ensure uniform vegetation characteristics in a passive microwave pixel with tens kilometers resolution. These limit the algorithm applied to the space-borne sensors on a considerable extent.

Additionally, aiming at developing a combined radar and radiometer algorithm for SMAP soil moisture retrieval, Das et al. [138] considered that the land vegetation and surface roughness factor vary on time scales longer than that those associated with soil moisture. In other words, the changes of radar or radiometer observations are only due to the soil moisture change over a short period of time. The increase of surface soil moisture will lead to decrease in radiometer and increase in radar measurements, and vice-versa. Therefore, over a short period of time the radar and radiometer measurements are expected to have functional relationship, and based on this a linear function was hypothesized. The unknown parameters slop and intercept of linear functional are dependent on the dominant vegetation and soil moisture characteristics. An intermediate resolution disaggregated brightness temperature field (9 km) was produced by blending fine-scale spatial heterogeneity detected by radar observations with coarser-scale radiometer (36 km) measurements. These disaggregated brightness temperatures are then used with established radiometer-based single channel algorithm to retrieve soil moisture at the intermediate resolution. The algorithm directly retrieves soil moisture from the intermediate resolution brightness temperature, and the low resolution soil moisture is not required. It effectively limits the error cumulative from low resolution to medium-resolution retrieved soil moisture. However the time scale of vegetation and surface roughness invariant was not defined clearly and the radiometer-based single-channel algorithm requires many ancillary data as input.

4 Microwave remote sensing of land surface temperature

Land surface temperature is also a key parameter in numerical weather-prediction model that leads to significant forecasting improvement in the physics of land surface processes on regional and global scales, combining the results of all surface-atmosphere interactions and energy fluxes between atmosphere and the ground. In the past twenty years, the rapid development of thermal infrared remote sensing technology provides a new way to quickly obtain the spatial information of surface temperature in regional scale, but thermal remote sensing is influenced much by clouds, atmospheric water vapor content, and rainfall. Over 60% areas in MODIS LST product are influenced by cloud and rainfall. Micro-wave remote sensing has advantage in these aspects because it can overcome these shortcomings of thermal remote sensing, such as cloud cover, smoke, and aerosol effects. So it becomes urgent to study how to use passive microwave data to retrieve land surface temperature.

In fact, it is very difficult to retrieve land surface temperature from passive microwave remote sensing data, because there are always the $N+1$ unknowns (N-emission rate and a surface temperature) for N frequency measurements of the thermal radiation, which is a typical ill-posed inversion problem. Moreover, the microwave emissivity is determined mainly by the dielectric constant, which is influenced by the physical temperature, salinity, moisture content, soil texture, and other factors (vegetation structure and type). These make the development of a common physical algorithm very difficult. Here two typical and representative works are introduced. Mcfarland et al. [139] did some research and analysis for retrieving land surface temperature from passive microwave SSM/I data. Although it is limited by the data acquisition, it got many useful conclusions. The impact of water must be corrected when there is water in the land surface. The high dielectric constant of water reduces the emissivity of 19 GHz, and the polarization of the radiation is very high for water, so the brightness temperature decreases and the difference of polarization between brightness temperature increases because of the surface water. The difference of brightness temperature between 37 and 19 GHz can be used to revise the impact. The water vapor has influence for the emission of the 37 GHz, so the difference of 37 and 22 GHz vertical polarization can be used to revise the radiation effects of atmospheric water vapor. Mao et al. [140] made the MODIS LST product as the large scale land surface data of the AMSR-E, which overcomes the difficulty in obtaining the large scale ground truth measurement of LST matching the pixel scale of passive microwave AMSR-E data at the satellite pass. This also provides an application for researching how to use multi-sensor to retrieve surface parameters and mutual correction. Three rep-

resentative surface types are selected as the study areas: Northeast China (forest), North Africa (desert), and Tibet (snow). In this research, the best single band to retrieve land surface temperature is found by regression analysis between MODIS LST product and brightness temperature of AMSR-E, and then the best method is also built through eliminating the influence of soil water and atmosphere water by simulation of AIEM model. The analysis showed that: the error is relatively large when the sample data from three typical regions are put together to make regression analysis; the retrieval accuracy will be greatly improved when the sample data from Tibet region are excluded. The main reason is due to the impact of snow and frozen. The surface radiation mechanism of snow and permafrost is different from others. The analysis also shows that the penetration of different microwave bands is different for the land surface and vegetation, which determines the satellite receiver to get different surface radiation energy. The influence of atmospheric water vapor, clouds and rain particle is the smallest for the low-frequency of microwave, so the 37 V (GHz) brightness temperature is most suitable for retrieving land surface temperature. In the absence of atmospheric scattering and re-radiation, high frequency has a lower dielectric constant of water and the thicker of light radiation compared with low frequency, and the regression analysis between the brightness of 89 V (GHz) and MODIS surface temperature products indicates that the correlation is the maximum. So the high frequency of vertical of the brightness temperature can improve the retrieval accuracy of surface temperature. In the local analysis, they found that the radiation mechanism is very different when the local surface temperature is different, especially when surface temperature is less than 273 K. In order to improve the retrieval accuracy, the retrieval algorithm should be built for different conditions, especially when the land surface temperature is fewer than 273 K. The land surface should be at least classified into three types: water covered surface, snow-covered surface, and non-water and non-snow-covered land surface. According to the different land surface temperature, the retrieval frame can be depicted as Figure 4.

The soil moisture, roughness and land surface temperature are changing with the weather, time and place, which makes the retrieval more complicated, because different combinations of these factors can form the same and different emissivity. The various physical parameters are not

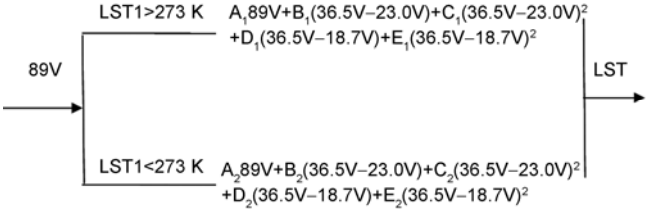

Figure 4 Flow chart of land surface temperature retrieval by passive microwave remote sensing.

isolated from each other. In order to take full advantage of the potential relationship between the geophysical parameters, Mao et al. [141] used multi-sensor/multi-resolution features of Earth Observing System (EOS/AQUA) and neural network to retrieve land surface temperature from passive microwave AMSR-E data. The analysis of simulation data by AIEM indicates that the neural network neural network can be used to retrieve land surface temperature from passive microwave, and the average error is under 2°C.

5 Vegetation parameters retrieval using microwave remote sensing

As one of the most active factors and principal parts in land ecosystem, vegetation accounts for more than half of land surface area. It plays an essential role in human living environment and provides abundant information to indicate the natural environment characteristics. Furthermore, vegetation is an important component of global carbon source and carbon sink and is indispensable in global water cycle. Remote sensing makes it possible and effective to monitor land surface vegetation in real time at global scale.

5.1 Vegetation parameters retrieval with passive microwave

Passive microwave sensors are sensitive to variations in vegetation properties in a relatively thick canopy. At present, there have been many studies on vegetation parameters retrieval based on passive microwave data. One commonly used tool in vegetation monitoring is remote-sensing-based index, which is an effective indicator of vegetation condition and has been successfully used for vegetation monitoring, soil moisture, and vegetation water content retrieval. As a result, it is significant and necessary to develop vegetation indices based on microwave remote sensing data to monitor vegetation more effectively. With decades of development, many vegetation indices from passive microwave instruments have been explored in previous studies, such as microwave polarization difference temperatures (MPDT) [142–145], Microwave Polarization Difference Index (MPDI) [146–148], and Microwave Vegetation Indices (MVIs) [149]. Some of them have been used widely in the related fields.

Early studies have shown that microwave polarization difference temperatures (MPDT) at 37 GHz NDVI were highly correlated to NDVI [130] and the relationship varied with the leaf water content [130, 150, 151]. According to microwave radiative transfer theory and field experiments, MPDT is related not only to vegetation properties but also to surface temperature, soil moisture, and roughness. To minimize the effect of physical temperature, Becker and Choudhury developed the normalized microwave polariza-

tion difference index (MPDI) [152]. MPDI can be described using the following formula $MPDI = c[T_b(V) - T_b(H)]/[T_b(V) + T_b(H)]$ for a given frequency, where C is a scale factor; $T_b(V)$ and $T_b(H)$ are the brightness temperatures of the given frequency in *H* and *V* polarization respectively. To some extent, MPDI can eliminate the effect of temperature.

Combining the data of microwave and thermal infrared, Paloscia and Pampaloni calculated the normalized brightness temperature, and developed a normalized brightness temperature difference between two frequencies (ΔT_n): $\Delta T_n = T_n(f_2) - T_n(f_1)$ [147]. It minimized the effect of temperature on vegetation properties and could be used to retrieve the biomass and vegetation water content.

Given the effects of soil parameters, such as soil moisture and roughness, the application of MPDI and ΔT_n in monitoring global vegetation was greatly restricted. Those vegetation indices can be used only when all the other parameters are uniform, which is impractical at microwave pixel scale. For a single microwave pixel, it is inevitable for the signals to be affected by different land conditions due to the coarse spatial resolution, which makes it an obstacle in the application in global vegetation monitoring. Njoku and Chan [153] proposed a parameter combining vegetation and soil roughness through analyzing multi-temporal AMSR-E data. The variation of this parameter was controlled mainly by vegetation water content. But this algorithm had many limitations in global application and only reflected the relative variation of vegetation.

Min and Lin [154] defined a new vegetation index, which combined the parameters of vegetation and roughness using multi temporal AMSR-E data. It was called the microwave emissivity difference vegetation index (EDVI) and showed by the formula $2\cdot[T_{bp}(f_1) - T_{bp}(f_2)]/[T_{bp}(f_1) + T_{bp}(f_2)]$. This index can be calculated by using brightness temperature of 19 and 37 GHz and can be used in dense forest directly without observation to the ground. It has shown that EDVI was more sensitive to evapotranspiration than NDVI and could be used in turbulent flux estimation.

Based on zero-order microwave radiative transfer model, Shi et al. [149] derived new passive microwave vegetation indices (MVIs) based on AMSR-E data. Different from those in the previous studies, MVIs were independent of soil emission signals and were related only to vegetation properties (Figure 5), such as vegetation coverage, biomass, temperature, size and geometry of vegetation components. Based on comparison between MVIs-B and vegetation water content from SMEX02, there was a good correlation with R^2=–0.8436. Hence, it can be inferred that MVIs-B is a good indicator of vegetation water content and has the potential of eliminating vegetation effect in soil moisture and

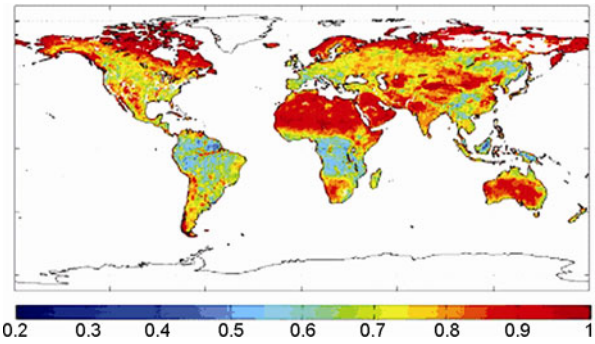

Figure 5 Monthly mean value for MVI in April, 2003.

vegetation water content retrieval process.

With the launch of L band sensor Soil Moisture and Ocean Salinity (SMOS), passive microwave remote sensing study of vegetation has stepped into a new period of single frequency and multiple angles. On the one hand, the L band data can be used to monitor thicker canopy and thereby enhance the ability to detect the ground information in forest land because of its greater penetrability compared with higher frequencies. On the other hand, SMOS provides new opportunities in global vegetation study due to its multi-angle information, which is different from traditional sensors. Chen et al. [155] has developed multi-angle vegetation index of L band through simulation using AIEM and analysis of theoretical model. Based on field experiment data analysis, it has shown that the index was highly corrected to LAI.

Besides, many studies on vegetation parameters retrieval are based on semi-empirical model or iterative algorithm directly without using vegetation indices. In the official land parameters retrieval algorithm of AMSR-E, vegetation water content can be calculated at the same time when soil moisture was retrieved based on radiative transfer theory using iterative algorithm. In this algorithm, the temperatures of vegetation, soil and environment were set to be equal. The contribution of outer space radiation was ignored and the upward radiation was the same as downward. It has been demonstrated that the daily product of vegetation water content with 60 km spatial resolution has an accuracy of 0.15 kg/m^2. Based on this study, Sahoo et al. [156] improved the hypothesis and the simplifying method and developed a new algorithm to retrieve soil moisture and vegetation water content. Wigneron et al. [157] proposed a method to retrieve crop water content through combining ω-τ model and a uniaxial crystal model, which was applied to thin stem canopy. In this study, optical depth τ was considered to be correlated to vegetation water content, so that we can minimize the difference between observed and simulated emissivity and then estimate vegetation water content. Chai et al. [158] has revealed the linear relationship between the absorbing component of optical depth and vegetation biomass by building a simulating database according to AMSR-E configuration. This work provided a new way

to retrieve biomass in the future research. On the basis of Chai's conclusion, Zhang et al. [159] has developed an algorithm to estimate the biomass of North-East Asian area using multi-angle information of SMOS with a new parameterized model. In that paper, he obtained structural parameters of different kinds of vegetation with the help of L system firstly, and used them as input of the first order radative transfer model for database simulation. Based on the simulation database, a multi-angle parameterized vegetation model was built and used to estimate the biomass. The R^2 was higher than 0.6 according to the referencing dataset. The research can be viewed as an exploration and preliminary application of passive microwave remote sensing in vegetation biomass estimation.

5.2 Vegetation parameters retrieval with active microwave

Although only worked for about 100 days, the SAR onboard Seasat opened a new era of remote sensing. SAR has the capability of working at all time and under all-weather conditions because it works on microwave and is active sensor. The research on space-borne and airborne SAR data shows that it has the potential for the retrieval of vegetation parameters especially over areas covered by cloud or fogs all year. A serial of SAR systems developed jointly by European Space Agency (ESA), Japanese space Agency (JAXA), Canadian Space Agency (CSA), and NASA accelerated the application of SAR data in the estimation of vegetation parameters.

Besides the characteristics of terrain objects, Radar backscattering is highly affected by system parameters including incidence angle, wavelength and polarization. Radar systems are designed using specific parameters according to its objectives. In the initial phase, SAR can only provide the backscattering coefficients. With the development of interferometric SAR technology, the interferometric coherence, which was initially used to evaluate the quality of InSAR data, was found to be correlated with terrain objects. According to the analysis method, the application of SAR data can be divided into two categories, i.e., qualitative and quantitative analysis. Qualitative analysis is mainly referred to image classification whereas quantitative analysis is quantitative estimation of parameters of vegetation structures. The vegetation parameters that can be estimated from SAR data include biomass, height and leaf area index (LAI). Therefore, this section will be extended to four aspects: (1) SAR classification; (2) estimation of biomass; (3) retrieval of vegetation height; (4) estimation of LAI.

5.2.1 SAR image classification

In the first stage of SAR application, SAR image classification is the main research directions. The classification was based mainly on multi-temporal, multi-frequency, multi-angle and multi-polarization data. Cimino et al. [160] explored the potential of forest classification using multi-angle data. The results showed that multi-angle data can be used to classify the forest composed of different species or single-species forest with different forest structures. Ranson et al. [161] tried forest classification using full polarization AIRSAR data of C, L and P bands acquired in winter (March 3) and summer (September 2). The results showed that with principal component analysis of temporal data sets (winter and late summer), SAR images can be classified into general forest categories such as softwood, hardwood, regeneration, and clearing with better than 80% accuracy. Other non-forest classes such as bogs, wetlands, grass, and water were also accurately classified. Classifications from single date images suffered in accuracy. The winter image had significant confusion of softwoods and hardwoods with a strong tendency to overestimate hardwoods. Modeling results suggest that increased double- bounce scattering of the radar beam from conifer stands because of lowered dielectric constant of frozen needles and branches was the contributing factor for the misclassifications. Pierce et al. [162] proposed a knowledge-based classification method of polarimetric SAR images. The classifier design uses knowledge of the nature of radar backscattering from surfaces and volumes to construct appropriate discriminator in a sequential format. The classifier used L and C band polarimetric SAR measurement of imaged scene to classify individual pixels into one of four categories: tall vegetation (trees), short vegetation, urban, or bare surfaces, with the last category encompassing water surfaces, bare soil surfaces and concrete or asphalt-covered surfaces. Among all cases and all categories, the classification accuracy ranged between 91% and 100%. The variables used in the classifier design include the backscattering coefficients $\sigma^0_{vv}(L)$, $\sigma^0_{hh}(L)$, $\sigma^0_{hv}(L)$, and the phase difference of co-polarization $\phi_{hh}-\phi_{vv}$. The classifier also used the textural information by computing the normalized variance for each pixel. By using 5×5 pixel window centered at the pixel of interest, the mean μ and standard deviation σ of 25 pixels are computed for each magnitude. The measured normalized variance for a given polarization is composed of components: a component due to speckle and a component due to scene texture (spatial inhomogeneity). The speckle variance is target-independent and is a function of the number of independent samples. The window size can be determined from knowledge of the multi-look processing algorithm or can be estimated directly from the image by calculation the variance for texture-less target such as a calm water surface. The speckle variance is the same for all polarizations. Given the normalized variance and the computed speckle variance, we can get the textural variance. In the knowledge-based classifier, the urban pixels are first separated from everything else. It is characterized by double-bounce reflection mechanism resulting in a co-polarized phase difference close to ±180°. Additionally, urban scenes

exhibit higher values of image texture than do other distributed targets. The tall vegetation can be separated by L band cross-polarization backscattering coefficients in the second step. C band cross-polarization and L band texture information can be used to discriminate low vegetation. Rignot et al. [163] separated five vegetation types using fully polarimetric SAR data acquired by AIRSAR dominated by 1) white spruce, 2) balsam poplar, 3) black spruce, 4) alder/willow shrubs, and 5) bog/fen/nonforest vegetation. Accuracy of forest classification is investigated as a function of frequency and polarization of the radar, as well as the forest seasonal state, which includes winter/frozen, winter/thawed, spring/flooded, spring/unflooded, and summer/dry conditions. Classifications indicate that C-band is a more useful frequency for separating forest types than L- or P-bands, and HV polarization is the most useful polarization at all frequencies. The highest classification accuracy, with 90 percent of forest pixels classified correctly, is obtained by combining L-band HV and C-band HV data acquired in spring as seasonal river flooding recedes and before deciduous tree species have leaves. Saatchi et al. [164] investigated the boreal forest classification using multi-frequency fully polarized AIRSAR data. A Bayesian maximum a posteriori classifier was applied. The results showed that SAR images can be classified into dominant forest types such as jack pine, black spruce, trembling aspen, clearing, open water, and three categories of mixed strands with better than 90% accuracy. The unispecies stands such as jack pine and black spruce are separated with 98% accuracy, but the accuracy of mixed coniferous and deciduous stands was low due to some confusing factors. Saatchi et al. [165] explored the potential use of space-borne polarimetric synthetic aperture radar (SAR) data in mapping land-cover types and monitoring deforestation in tropics. A supervised Bayesian classifier designed for SAR signal statistics is employed to separate five classes: primary forest, secondary forest, pasture-crops, quebradao, and disturbed forest. The L- and C-band polarimetric SAR data acquired during the shuttle imaging radar-C (SIR-C)/X-SAR space-shuttle mission in 1994 are used as input data to the classifier. The SAR data can delineate these five classes with approximately 72% accuracy. The confusion arises when separating old secondary forests from primary forest and the young ones from pasture-crops. When the number of land-cover types was reduced to three classes including primary forest, pasture-crops, and re-growth-disturbed forest, the accuracy of classification increased to 87%. Comparison of SIR-C data acquired in April (wet period) and October (dry period) indicates that multi-temporal data can be used for monitoring deforestation; however, the data acquired during the wet season are not suitable for accurate land-cover classification. Simard et al. [166] investigated the use of a decision tree classifier and multi-scale texture measures to extract thematic information on the tropical vegetation cover from the Global Rain Forest Mapping (GRFM) JERS-1 SAR mosaics. They focused on a coastal region of Gabon. The analysis proves that the radar backscatter amplitude is important for separating basic land cover categories such as savannas, forests, and flooded vegetation. Texture is found to be useful for refining flooded vegetation classes. Temporal information from SAR images of two different dates is explicitly used in the decision tree structure to identify swamps and temporarily flooded vegetation. Lee et al. [167] addresses the application of polarization combinations in the crop and tree age classification. The results showed that L-Band fully polarimetric SAR data are best for crop classification, but P-Band is best for forest age classification. For dual polarization classification, the HH and VV phase difference is important for crop classification but less important for tree age classification. Also, for crop classification, the L-Band complex HH and VV can achieve correct classification rates almost as good as for full polarimetric SAR data, and for forest age classification, P-Band HH and VV should be used in the absence of fully polarimetric data. In all cases, multifrequency of fully polarimetric SAR is highly desirable.

The methods described above are based mainly on the backscattering coefficients of multi-temporal and multi-frequency and image textures. Cloude et al. [168] proposed an entropy-based classification scheme for land applications of polarimetric SAR. The classical classification method divided the pixels into specific forest types whereas in the new method pixels were classified by their scattering mechanisms according to their position in the alpha-H plane. This led to the application of polarization decomposition on the land cover classification. Lee et al. [169] proposed an algorithm using a combination of a scattering model-based decomposition developed by Freeman and Durden and the maximum likelihood classifier based on the complex Wishart distribution. The first step is to apply the Freeman and Durden decomposition to divide pixels into three scattering categories: surface scattering, volume scattering, and double-bounce scattering. To preserve the purity of scattering characteristics, pixels in a scattering category are restricted to be classified with other pixels in the same scattering category. An efficient and effective class initialization scheme is also devised to initially merge clusters from many small clusters in each scattering category by applying a merge criterion developed based on the Wishart distance measure. Then, the iterative Wishart classifier is applied. The stability in convergence is much superior to that of the previous algorithm using the entropy/anisotropy/Wishart classifier. Shimoni et al. [170] investigated the complementarity and fusion of different frequencies (L- and P-band), polarimetric SAR (PolSAR) and polarimetric interferometric (PolInSAR) data for land cover classification. A two-level fusion method was developed: Logistic regression (LR) as 'feature-level fusion' and the neural-network (NN) method for higher level fusion. For comparison, a support vector machine (SVM) was also applied. The results show that for both NN and SVM, the overall accuracy for each of

the fused sets is better than the accuracy for the separate feature sets. Moreover, fused features from different SAR frequencies are complementary and adequate for land cover classification, PolInSAR is complementary to PolSAR information, and both are essential for producing accurate land cover classification. Lardeux et al. [171] used a support vector machine (SVM) algorithm to assess the potential of radar data for tropical vegetation cartography. The contribution of the different polarimetric indicators is estimated through a greedy forward and backward method. The results are compared to those obtained with the standard Wishart approach. It is shown that, when radar data do not satisfy the Wishart distribution, the SVM algorithm performs much better than the Wishart approach. Sánchez-Lladó et al. [172] proposed the use of Deterministic Simulated Annealing (DSA) for Synthetic Aperture Radar (SAR) image classification for cluster refinement. They used the initial classification provided by the maximum-likelihood classifier based on the complex Wishart distribution that is then supplied to the DSA optimization approach. Entezari et al. [173] applied a classification algorithm based on the SVMs technique to the fully polarimetric AIRSAR L-band data. Several parameters are extracted from SAR data, including the individual channel backscatter value, Pauli decomposition coefficients, Krogager decomposition coefficients, and eigenvector decomposition parameters. Different combinations of polarimetric parameters are considered to assess the accuracy of the classification results. The accuracy of the SVMs is then compared with that obtained from several conventional classifiers, including the Maximum Likelihood classifier, Minimum Distance classifier, Mahalanobis Distance classifier, and Wishart classifier. The accuracy analysis shows that, for classification of fully polarimetric data, SVMs perform more poorly than the Wishart classifier whereas they perform better than the Maximum Likelihood, Minimum Distance, and Mahalanobis Distance classifiers. Moreover, the highest accuracy is achieved by using the coefficients of Krogager decomposition in the classification procedure. Mishra et al. [174] carried out the eigen value decomposition and Pauli decomposition to separate classes on the basis of their scattering mechanisms. This work is carried out by decision tree classification that uses the knowledge-based approach. It has been demonstrated quantitatively that standard polarimetric parameters such as polarized backscatter coefficients (linear, circular and linear 45°), co- and cross-pol ratios for both linear and circular polarizations can be used as information-bearing features for making decision boundaries. The classifier uses these data to classify individual pixel into one of the five categories: water, tall vegetation, short vegetation, urban and bare soil surface. The quantitative results shown by this classifier gives classification accuracy of about 88%. Haddadi et al. [175] presented an algorithm to extract optimized features of POLSAR images that are required for classification. The proposed algorithm involves three main steps: (i) feature extraction using decomposition algorithms, including both coherent and incoherent decomposition algorithms; (ii) feature selection using a combination of a genetic algorithm (GA) and an artificial neural network (ANN); and (iii) image classification using the neural network. The classification results obtained by the GA-based feature selection method exhibit the highest accuracy. Qi et al. [176] proposed a new four-component algorithm for land use and land cover (LULC) classification. These four components are polarimetric decomposition, PolSAR interferometry, object-oriented image analysis, and decision tree algorithms. First, polarimetric decomposition can be used to support the classification of PolSAR data. It is aimed at extracting polarimetric parameters related to the physical scattering mechanisms of the observed objects. Second, PolSAR interferometry is used to extract polarimetric interferometric information to support LULC classification. Third, the main purposes of object-oriented image analysis are delineating image objects, as well as extracting various textural and spatial features from image objects to improve classification accuracy. Finally, a decision tree algorithm provides an efficient way to select features and implement classification. The results indicate that the proposed method exhibits much better performance than the Wishart supervised classification for LULC classification. It indicates that all the four components have important contributions to the classification. Polarimetric information has significant implications for identifying different vegetation types and distinguishing between vegetation and urban/built-up. The polarimetric interferometric information is important in reducing the confusion between urban/built-up and vegetation and that between barren/sparsely vegetated land and vegetation. Object-oriented image analysis is very helpful in reducing the effect of speckle in PolSAR images by implementing classification based on image objects. The accuracy of the decision tree algorithm is similar to that of the support vector classification. Compared with the nearest neighbor and support vector classification, the decision tree algorithm is more efficient in selecting features and implementing classification. Furthermore, the decision tree algorithm can provide clear classification rules that can be easily interpreted based on the physical meaning of the features used in the classification.

5.2.2 Vegetation biomass estimation

Compared to optical data, SAR has great potential in the estimation of vegetation biomass because it can penetrate further into vegetations. Therefore it has been a hotspot in research. Toan et al. [177] investigated the relationship between red pine biomass and L and P band backscattering coefficients. The most striking observation has been the strong correlation of P-band backscatter intensity to forest biomass. Dobson et al. [178] examined the dependence of radar backscatter on aboveground biomass of mono specie conifer forests using polarimetric airborne SAR data at P-,

L- and C-bands. Radar backscatter is found to increase approximately linearly with increasing biomass until it saturates at a biomass level that depends on the radar frequency. The biomass saturation level is about 200 tons/ha at P-band and 100 tons/ha at L-band, and the C-band backscattering coefficient shows much less sensitivity to total aboveground biomass. Beaudoin et al. [179] went a step further in the understanding of the observations, using theoretical modeling applied to calibrated SAR data to explain the radar backscatter from the forest canopy under study. The study is presented at P band, which was found to be an optimal frequency band for forest observations. It was found that the HH return is physically related to both trunk and crown biomass, whereas VV and particularly HV returns are linked to crown biomass. Rignot et al. [180] found that at P-band HV-polarization, the error in predicted biomass is about 30% of the actual biomass. Errors obtained using L-band data are a few percents larger. These errors are caused by uncertainties in actual stand biomass estimates, significant inner-stand spatial variations in biomass, unusual conditions of forest stands following natural disturbances, along with interactions of the radar signals with a complex three-dimensional structure of the canopy. Multiple incidence angle data reveal that the incidence angle of the radar illumination is also a factor influencing the retrieval of biomass, even at HV-polarization, when it is larger than 50° or smaller than 25°. Finally, the radar response of the forest, and thereby the regression curves for biomass retrieval, is dependent on the seasonal and environmental conditions. Harrell et al. [181] examined the relationship between forest biomass and C band ERS-1 data and L-band JERS-1 data. Results indicate both ERS-1 and JERS-1 backscatter is responsive to biomass, density, and height, though other factors, principally surface moisture conditions, often have a stronger influence. Sensitivity to forest biomass and structure appears the greatest when surface moisture conditions are minimized as a factor. Biomass correlations with the radar backscatter were the strongest in the late winter Imagery when all sites had a snow cover, and late summer when the surface is mostly dry. ERS-1 data may be more sensitive to surface moisture conditions than the JERS-1 data due to the shorter wavelength of the C-band sensor.

Imhoff [182] believed that stand level forest canopy structure as measured by the size, density, and distribution of the stems, branches, and leaves may have a strong effect on SAR backscatter. The Michigan Microwave Canopy Scattering model (MIMICS) and forest canopy biometric data from tropical and subtropical broadleaf forests are used to simulate a series of forest stands having equivalent above ground biomass while still exhibiting substantial structural differences. Results indicate that structure can have a considerable effect on the SAR return for forests with equivalent above-ground biomass. Differences in backscatter of up to 18 dB were predicted for some bands and polarizations. A forest canopy structural descriptor derived from the vegetation surface area to volume ratio (SA/V), which is a measure of structural consolidation, appears to explain the differences in backscatter. Kasischke et al. [183] developed a method using total stem biomass to estimate the other components, with a total stem biomass being estimated from the radar image intensity values. Pulliainen et al. [184] investigated the seasonal changes of the C-band backscattering properties of boreal forests by applying a semi-empirical forest backscattering model and multi-temporal ERS-1 SAR data. The results show that the correlation between the backscattering coefficient and forest stem volume (biomass) varies from positive to negative depending on canopy and soil moisture. Additionally, the seasonal snow cover and soil freezing/thawing effects cause drastic changes in the radar response. Foody et al. [185] related SIR-C SAR data to the above-ground biomass of regenerating tropical forests in Amazonia, Brazil. C- and L-band SAR data in the conventional polarization configurations showed no significant relationship with forest biomass. However, the strength of the relationships was increased through the use of backscatter ratios and stratification of the forests by dominant species. They also demonstrate that an ability to differentiate between forests of different species composition, and canopy geometry, increases the strength of the relationship between the SAR backscatter and biomass. Harrell et al. [186] valuated various techniques for estimating aboveground woody plant biomass in pine stands found in the southeastern United States, using C- and L-band multiple polarization radar imagery collected by the Shuttle Imaging Radar-C (SIR-C) system. The LHV channel is the critical element in all the biomass equations. The addition of other channels, generally CHV or CHH, significantly improves biomass estimates, whether as a ratio or as additional terms in a regression equation. In these researches, the relationship between forest biomass and SAR data was based mainly on the statistical regression between field measurement and SAR signals. As described in the previous sections, many theoretical models of forest radar backscattering have been developed. Considering the accessibility and time consuming of field measurement, Ranson et al. [187] explored the feasibility of forest biomass estimation through the combination of forest growth model and 3D radar backscattering model. The regression relationship was built using simulated biomass and backscattering coefficients. It was further calibrated by field measurement. Ranson et al. [188] explored the effect of frozen and freezing on SAR backscattering. Simple linear regression models relating measured above-ground woody biomass to SIR-C backscatter were not the same, but statistical tests showed that the slopes were not significantly different, suggesting that a simple correction by an offset is possible. Besides the effect of environmental factors and saturation problems, terrain is another import problem in SAR application. It can introduce calibration error and change the scattering mechanism. Sun et al. [189] simulated the effects of terrain using

3D radar backscattering model. A regression model between local incidence angle and backscattering was built using simulated dataset and applied to the image correction. The results showed that the correction can improve the biomass estimation accuracy. Kimes et al. [190] used a neural network approach to develop accurate algorithms for inverting a complex forest backscatter model. The model combines a forest growth model with a radar backscatter model. By using the simulated data, various neural networks were trained with inputs of different backscatter bands. The networks that used only AIRSAR bands (C, L, P) had a high degree of accuracy. The inclusion of the X band with the AIRSAR bands did not seem to significantly increase the accuracy of the networks. In the networks that have only the L band or only C band, poor accuracies were obtained. Frate et al. [191] also tried the estimation of forest biomass using neural network approach and L, P band data. Look Up Table (LUT) is also one of the method for the inversion of theoretical model. It is mostly applied in optical model. Ni et al. [192] investigated the biomass estimation using LUT and radar backscattering through the combination of forest growth model and 3D radar backscattering model. Two types of searching methods i.e., Nearest Distance (ND) and Distance Threshold (DT) were elevated. The results showed that DT was superior to ND.

The studies described in previous part are based mainly on the radar backscattering. Besides radar backscattering coefficients, interferometric SAR coherence is another variable provided by SAR data. It was initially used to evaluate the quality of InSAR pairs. Some researchers found that it was also correlated with the characteristics of terrain objects. Luckman et al. [193] examined the relationship between forest biomass and biomass using ERS-1/2 tandem data with 44 days time intervals and JERS data with 132 days time intervals. The results showed it can obviously provide more information about tropical forest. Gaveau [194] simulated the relationship between forest biomass and coherence of ERS-1/2 at boreal forest. The results showed that the temporal decorrelation is the main decoherence factor. The more biomass is the less stable of scatters. Santoro et al. [195] develop the water-cloud model into coherent version and apply it into the stem volume (biomass=stem volume × density factor) estimation. Santoro et al. [196] analyzed the correlation of multi-temporal coherence and stem volume and found that the coherence of forest covered by snow is more stable and suitable for the estimation of forest stem volume.

5.2.3 Retrieval of vegetation height

Another observation provided by interferometric SAR is the InSAR phase. Scientist tried to use the interferometric phase information to estimate forest height. Hagberg et al. [197] examined the boreal forest height information contained in InSAR phase in winter. They believed that four requirements are need for the estimation of forest height from InSAR data: (1) the wavelength is short enough to guarantee that the scattering phase center is near the forest canopy top; (2) the ground elevation under forest should be known; (3) the baseline should be long enough because the longer baseline is more sensitive to forest height variation; (4) scatter should be stable at wavelength scale to minimize the influence of temporal decoherence. Pang et al. [198] tried the effective forest height estimation using C and L band data of SIR-C/X-SAR and found that forest height information is contained in the digital elevation model derived from interferometric SAR data. Different wavelength is preferred for different forest stands. The short wavelength is good for uniform forest whereas the longer wavelength is better for heterogeneous forest. The accuracy of ground elevation can be affected by ground control points. The difference between forest stand and clear cuts is useful for the estimation of forest height. These studies are based mainly on single polarization. Polarimetric SAR interferometry becomes a new technology in the estimation of forest height. Polarization is sensitive to the shape and directions of scatters. The interaction process is different for different polarization. For example, cross-polarization mainly comes from forest canopy whereas co-polarization mainly comes from ground contribution. The combination of polarization and interferometry provide a new way for the estimation of forest height. Cloude et al. [199] proposed the concept of polarimetric SAR interferometry (PolInSAR). Its main idea is that the coherence is first optimized through the polarization combination. Then the scattering components coming from different part of forest are separated through polarization decomposition. Papathanassiou et al. [200] proposed a method for the extraction of vegetation vertical structure using single baseline PolInSAR data. They supposed that the backscattering from forest canopy has no specific polarization feature. A theoretical model of complex coherence was derived from Random volume on Ground (RVOG) forest scene. Forest heights are estimated through the iterative solution of the model. The parameters needed to be set in the model include vegetation height, ground phase, canopy attenuation, and the ratio between contributions from ground and canopy on each polarization. Therefore its computation load is heavy because it in fact is a computation in six dimensional spaces. Cloude et al. [201] proposed a three-step inversion method based on the geometry of the RVOG model. The linear fitting over unit circle on complex coherence plane accomplished using the least square multiply. The ground phase was estimated using the fitted line. The vegetation height and attenuation were estimated finally through Look Up Table method. Yamada et al. [202] introduced the ESPRIT (Estimation of Signal Parameters via Rotational Invariance Techniques) into the estimation of forest height using PolInSAR data. It improves the computation efficiency and provides the reliable scattering phase from forest canopy [203]. Cloude [204] further proposed polarization coherence tomography. Given the vegetation

height and ground phase, the vertical profile function of vegetation can be constructed through the Legendre-Fourier expansion.

5.2.4 Estimation of Leaf area index

Leaf area index is one of the key parameters that can be estimated using optical image. However, in some special areas, it is difficult to acquire optical image due to the coverage of cloud and fogs. Some research tried to estimate LAI using SAR data. Paloscia [205] analyzed the sensitivity of multi-frequency multi polarization SAR data to crop LAI and found that L band data are sensitive to some types of crops. Manninen et al. [206] tried to use VV/HH of ENVISAT-ASAR to estimate the LAI of boreal forest. The results showed that the overall estimation accuracy is 0.27. Chen et al. [207] examined the relationship between VV/HH of ASAR data and rice LAI using radiative transfer model. The estimation accuracy is 0.17.

6 Conclusions

With the advances of remote sensing science, remote sensing, especially microwave remote sensing, will play a more and more important role in the studies of global water, carbon and energy cycles. It is necessary to establish the observation and inversion platform based on the integration of the observations from multiple data sources and optimization of different inversion algorithms in order to produce long time-series remote sensing products at a higher accuracy and spatial resolutions for the study of earth system processes.

This work was supported by National Natural Science Foundation of China (Grant Nos. 40930530 and 40901180).

1 Shen J, Maradudin A A. Multiple scattering of waves from random rough surfaces. Phys Rev B, 1980, 22: 4234–4240
2 Bahar E. Full wave solutions for the depolarization of the scattered radiation fields by rough surfaces of arbitrary slope. IEEE Trans Antennas Propag, 1981, 29: 443–454
3 Voronovich A G. Small-slope approximation in wave scattering by rough surfaces. Soviet Phys-JETP, 1985, 62: 65–70
4 Fung A K, Li A Q, Chen K S. Backscattering from a randomly rough dielectric surface. IEEE Trans Geosci Remote Sensing, 1992, 30: 356–369
5 Milder D M. An improved formalism forwave scattering from rough surfaces. J Acoust Soc Amer, 1991, 89: 529–541
6 Licheri M, Floury N, Borgeaud M, et al. On the scattering from natural surfaces: The IEM and the improved IEM. Proceeding of IGARSS, 2001. 2911–2913
7 Hsieh C Y, Fung A K, Nesti G, et al. A further study of the IEM surface scattering model. IEEE Trans Geosci Remote Sensing, 1997, 35: 901–909
8 Alvarez-Perez J L. An extension of the IEM/IEMM surface scattering model. Waves Random Med, 2001, 11: 307–329
9 Fung A K, Liu W Y, Chen K S. A Comparison Between IEM-based Surface Bistatic Scattering Models. Proceeding of IGARSS, 2002. 441–443
10 Chen K S, Wu T D, Tsay M K, et al. A note on the multiple scattering in an IEM model. IEEE Trans Geosci Remote Sensing, 2000, 38: 249–256
11 Chen K S, Wu T D, Tsang L, et al. The emission of rough surfaces calculated by the integral equation method with a comparison to a three-dimensional moment method simulations. IEEE Trans Geosci Remote Sensing, 2003, 41: 90–101
12 Du Y. A new bistatic model for electromagnetic scattering from randomly rough surfaces. Waves Random Compl Med, 2008, 18: 109–128
13 Tsang L, Kong J A, Shin R T. Theory of Microwave Remote Sensing. Wiley Interscience, 1985
14 Tsang L, Kong J A, Ding K H. Scattering of Electromagnetic Waves: Theories and Applications. Wiley, 2000
15 Tsang L, Chen C, Chang A T, et al. Dense media radiative transfer theory based on quasicrystalline approximation with applications to passive microwave remote sensing of snow. Radio Sci, 2000, 35: 731–749
16 Tsang L, Pan J, Liang D, et al. Modeling active microwave remote sensing of snow using dense media radiative transfer (DMRT) theory with multiple-scattering effects. IEEE Trans Geosci Remote Sensing, 2007, 45: 990–1004
17 Xu X, Liang D, Tsang L, et al. Active remote sensing of snow using NMM3D/DMRT and comparision with CLPX II airborne data. IEEE J Selected Top Appl Earth Observ Remote Sensing, 2010, 3: 689–697
18 Stogryn A. A study of the microwave brightness temperature of snow from the point of view of strong fluctuation theory. IEEE Trans Geosci Remote Sensing, 1986, 24: 220–231
19 Shi J, Jiang L, Zhang L, et al. A parameterized multifrequency polarization surface emission model. IEEE Trans Geosci Remote Sensing, 2005, 43: 2831–2841
20 Jiang L, Shi J, Tjuatja S, et al. A parameterized multiple-scattering model for microwave emission from dry snow. Remote Sens Environ, 2007, 111: 357–366
21 Du J, Shi J, Rott H. Comparison between a multi-scattering and multi-layer snow scattering model and its parameterized snow backscattering model. Remote Sens Environ, 2010, 114: 1089–1098
22 Pulliainen J T, Grandell J, Hallikainen M T. HUT snow emission model and its applicability to snow water equivalent retrieval. Trans Geosci Remote Sensing, 1999, 37: 1378–1390
23 Hallikainen M T, Ulaby F T, Vandeventer T E. Extinction behavior of dry snow in the 18- to 90-GHz range. Trans Geosci Remote Sensing, 1987, 6: 737–745
24 Wiesmann A, Mätzler C. Microwave emission model of layered snowpacks. Remote Sens Environ, 1999, 70: 307–316
25 Wiesmann A, Mätzler C, Weise T. Radiometric and structural measurements of snow samples. Radio Sci, 1998, 33: 273–289
26 Ding K H, Xu X, Tsang L. Electromagnetic scattering by bicontinuous random microstructures with discrete permittivities. IEEE Trans Geosci Remote Sensing, 2010, 48: 3139–3151
27 Berk N F. Scattering properties of the leveled-wave model of random morphologies. Phys Rev A, 1991, 44: 50–69
28 Lang R H. Electromagnetic backscattering from a sparse distribution of lossy dielectric scatterers. Radio Sci, 1981, 16: 15–30
29 Ulaby F T, Elachi C. Radar Polarimetry for Geoscience Applications. Artech House, 1980
30 Karam M A, Fung A K, Lang R H, et al. A microwave scattering model for layered vegetation. IEEE Trans Geosci Remote Sensing, 1992, 30: 767–784
31 Sun G, Ranson K J. A three-dimensional radar backscatter model of forest canopies. IEEE Trans Geosci Remote Sensing, 1995, 33: 372–382
32 Ni W J, Guo Z F, Sun G Q. Improvement of a 3D radar backscattering model using matrix-doubling method. Sci China Ser D-Earth Sci, 2010, 53: 1029–1035
33 Stiles J M, Sarabandi K. A scattering model for thin dielectric cylinders of arbitrary crosssection and electrical length. IEEE Trans Antennas Propag, 1996, 44: 260–266

34 Karam M A, Fung A K, Antar Y M. Electromagnetic wave scattering from some vegetation samples. IEEE Trans Geosci Remote Sensing, 1988, 26: 799–808
35 Waterman P C. Matrix formulation of electromagnetic scattering. Proc IEEE, 1965, 53: 805–812
36 Mishchenko M I, Travis L D. T-matrix computations of light scattering by large spheroidal particles. Opt Commun, 1994, 109: 16–21
37 Mishchenko M I, Travis L D, Macke A. Scattering of light by polydisperse, randomly oriented, finite circular cylinders. Appl Opt, 1996, 35: 4927–4940
38 Wielaard D J, Mishchenko M I, Macke A, et al. Improved T-matrix computations for large, nonabsorbing and weakly absorbing nonspherical particles and comparison with geometrical-optics approximation. Appl Optics, 1997, 36: 4305–4313
39 Macelloni G, Nesti G, Pampaloni P, et al. Experimental validation of surface scattering and emission models. IEEE Trans Geosci Remote Sensing, 2000, 38: 459–469
40 Barber P W. Resonance electromagnetic absorption by nonspherical dielectric objects. IEEE Trans Geosci Remote Sensing, 1977, 25: 373–381
41 Iskander M F, Lakhtakia A, Durney C H. A new procedure for improving the solution stability and extending the frequency range of the EBCM (Extended Boundary Condition Method for EM absorption and scattering in biological dielectric objects). IEEE Trans Antennas Propag, 1983, 31: 317–324
42 Kahnert F M. Numerical methods in electromagnetic scattering theory. J Quanti Spectr Rad Transfer, 2003, 79–80: 775–824
43 Al-Rizzo H M, Tranquilla J M. Electromagnetic wave scattering by highly elongated and geometrically composite objects of large size parameters: The generalized multipole technique. Appl Optics, 1995, 34: 3502–3521
44 Doicu A, Wriedt T. Calculation of the T matrix in the null-field method with discrete sources. Opt Soc Amer, 1999, 16: 2539–2544
45 Yan W Z, Du Y, Wu H, et al. EM scattering from a long dielectric circular cylinder. Prog Electromag Res, 2008, 85: 39–67
46 Yan W Z, Du Y, Li Z Y, et al. Characterization of the validity region of the extended T-matrix method for scattering from dielectric cylinders with finite length. Prog Electromag Res, 2009, 96: 309–328
47 Koh I S, Sarabandi K. A new approximate solution for scattering by thin dielectric disks of arbitrary size and shape. IEEE Trans Antennas Propag, 2005, 53: 1920–1926
48 Chiu T, Sarabandi K. Electromagnetic scattering from short branching vegetation. IEEE Trans Geosci Remote Sensing, 2000, 38: 911–925
49 Davidson M W, Toan T L, Mattia F, et al. On the characterization of agricultural soil roughness for radar remote sensing studies. IEEE Trans Geosci Remote Sensing, 2000, 38: 630–640
50 Roo R D, Du Y, Ulaby F, et al. A semi-empirical backscattering model at L-band and C-band for a soybean canopy with soil moisture inversio. IEEE Trans Geosci Remote Sensing, 2001, 39: 864–872
51 Rodriguez E. Beyond the Kirchhoff approximation II electromagnetic scattering. Radio Sci, 1991, 26: 121–132
52 Toan T L, Ribbes F, Wang L F, et al. Rice crop mapping and monitoring using ERS-1 data based on experiment and modeling results. IEEE Trans Geosci Remote Sensing, 1997, 35: 41–56
53 Wigneron J P, Calvet J C, Kerr Y, et al. Microwave emission of vegetation: Sensitivity to leaf characteristics. IEEE Trans Geosci Remote Sensing, 1993, 31: 716–726
54 Wigneron J P, Calvet J C, Chanzy A, et al. A composite discrete-continuous approach to model the microwave emission of vegetation. IEEE Trans Geosci Remote Sensing,1995, 33: 201–211
55 Stiles W H, Ulaby F T, Rango A. Microwave measurements of snowpack properties. Nord Hydrol, 1981, 12: 143–166
56 Armstrong R L, Chang A T C, Rango A, et al. Snow depth and grain size relationships with relevance for passive microwave studies. Annals Glaciol, 1993, 17: 171–176
57 Hofer R, Mätzler C. Investigation of snow parameters by radiometry in the 3- to 60-mm wavelength region. J Geophys Res, 1980, 85: 453–460
58 Rott H, Sturm K. Microwave signature measurements of Antarctic and Alpine snow. Proc 11th EARSeL Symp, Graz, Austria, 1991. 140–151
59 Hallikainen M, Ulaby F T, Deventer T E. Extinction Behavior of Dry Snow in the 18 to 90 GHz Range. IEEE Trans Geosci Remote Sensing, 1987, 25: 737–745
60 Ulaby F T, Moore R K, Fung A. Microwave Remote Sensing. MA: Addison-Wesley-Longman, 1981
61 Matzler C. Applications of the interaction of microwaves with the natural snow cover. Remote Sensing Rev, 1987, 2: 259–391
62 Tsang L. Dense media radiative transfer theory for dense discrete random media with particles of multiple sizes and permittivities. Prog Electromag Res, 1992, 5: 181–225
63 Wiesmann A, Matzler C, Weise T. Radiometric and structural measurements of snow samples. Radio Sci, 1998, 33: 273–289
64 Brogioni M, Macelloni G, Palchetti E, et al. Monitoring snow characteristics with ground-based multifrequency microwave radiometry. IEEE Trans Geosci Remote Sensing, 2008, 47: 3643–3655
65 Kurvonen L, Hallikainen M T. Influence of Land-cover category on brightness temperature of snow. IEEE Trans Geosci Remote Sensing, 1997, 35: 367–377
66 Kruopis N, Praks J, Arslan A N, et al. Passive microwave measurements of snow-covered forest areas in EMAC'95. IEEE Trans Geosci Remote Sensing, 1999, 37: 2699–2705
67 Stankov B, Cline D, Weber B, et al. High-resolution airborne polarimetric microwave imaging of snow cover during the NASA cold land processes experiment. IEEE Trans Geosci Remote Sensing, 2008, 46: 3672–3693
68 Chang A T C, Foster J L, Hall D K. Nimbus-7 SMMR derived global snow cover parameters. Annals Glaciol, 1987, 9: 39–44
69 Rango A, Martine J, Chang A T C, et al. Average areal water equivalent of snow in a mountain basin using microwave and visible satellite data. IEEE Trans Geosci Remote Sensing, 1989, 27: 740–745
70 Goodison B, Walker A. Canadian development and use of snow cover information from passive microwave satellite data. In: Choudhury B, Kerr Y, Njoku E, eds. Passive Microwave Remote Sensing of Land-Atmosphere Interactions. Utrecht: VSP BV, 1994. 245–262
71 Chang A T C, Grody N, Tsang L, et al. Algorithm Theoretical Basis Document (ATBD) for AMSR-E Snow Water Equivalent Algorithm. NASA/GSFC, November 1997
72 Foster J L, Chang A T C, Hall D K. Comparison of snow mass estimation from a prototype passive microwave algorithm, a revised algorithm and a snow depth climatology. Remote Sens Environ, 1997, 62: 132–142
73 Pulliainen J T, Grandell J, Hallikainen M T. HUT snow emission model and its applicability to snow water equivalent retrieval. IEEE Trans Geosci Remote Sensing, 1999, 37: 13782–1390
74 Rango A, Chang A T C, Foster J L. The utilization of spaceborne microwave radiometers for monitoring snowpack properties. Nord Hydrol, 1979, 10: 25–40
75 Kunzi K F, Patil S, Rott H. Snow-cover parameters retrieved from Nimbus-7 scanning multichannel microwave radiometer (SMMR) data. IEEE Trans Geosci Remote Sensing, 1983, 20: 452–467
76 Aschbacher J. Land surface studies and atmospheric effects by satellite microwave radiometry. Ph D Dissertation. University of Innsbruck, 1989
77 Foster J L, Sun C, Walker J P, et al. Quantifying the uncertainty in passive microwave snow water equivalent observations. Remote Sens Environ, 2005, 94: 187–203
78 Derksen C, Walker A, Goodison B. A comparison of 18 winter seasons of *in situ* and passive microwave derived snow water equivalent estimates in Western Canada. Remote Sens Environ, 2003, 88: 271–282
79 Derksen C. The contribution of AMSR-E 18.7 and 10.7 GHz measurements to improved boreal forest snow water equivalent retrievals. Remote Sens Environ, 2008, 112: 2700–2709
80 Derksen C, Toose P, Rees A, et al. Development of a tundra-specific

snow water equivalent retrieval algorithm for satellite passive microwave data. Remote Sens Environ, 2010, 114: 1699–1709
81 Cao S M, Li P J, Robinson D A. Evaluation and application of SMMR Remote Sensing of China western snow (in Chinese). Environment Remote Sensing, 1993, 8: 260–269
82 Cao S M, Li P J. Microwave remote sensing of China western snow (in Chinese). J Mountain Res, 1994, 12: 230–234
83 Che T, Li X. Development and prospect of estimating snow water equivalent: Using passive microwave remote sensing data. Adv Earth Sci, 2004, 2: 204–210
84 Sun Z W, Shi J, Jiang L M, et al. Development of snow depth and snow water equivalent algorithm in Western China using passive microwave remote sensing data. Adv Earth Sci, 2006, 21: 1364–1369
85 Chang S. Researches on the Improvements of the Passive Microwave Inversion Algorithm for snow in China Region (in Chinese). Master Thesis. Beijing: Beijing Normal University, 2006
86 Wang P. Improvements on FY3/MWRI Passive Microwave Snow Inversion Algorithm for China Region (in Chinese). Master Thesis. Beijing: Beijing Normal University, 2011
87 Kelly R E, Chang A T, Tsang L, et al. A prototype AMSR-E global snow area and snow depth algorighm. IEEE Trans Geosci Remote Sensing, 2003, 41: 1–13
88 Josberger E G, Mognard N M. A passive microwave snow depth algorithm with a proxy for snow metamorphism. Hydrol Processes, 2002, 16: 1557–1568
89 Grippa M, Mognard N, Toan T L, et al. Siberia snow depth climatology derived from SSM/I data using a combined dynamic and static algorithm. Remote Sens Environ, 2004, 93: 30–41
90 Roy V, Goita K, Royer A, et al. Snow water equivalent retrieval in a Canadian boreal environment from microwave measurements using the HUT snow emission model. IEEE Trans Geosci Remote Sensing, 2004, 42: 1850–1858
91 Jiang L M, Shi J, Tjuatja S, et al. Estimation of snow water equivalence using the polarimetric scanning radiometer from the Cold Land Processes Experiments (CLPX03). IEEE Trans Geosci Remote Sensing Lett, 2011, 8: 359–363
92 Davis D T, Chen Z X, Hwang J N, et al. Retrieval of snow parameters by iterative inversion of a neural-network. IEEE Trans Geosci Remote Sensing, 1993, 31: 842–852
93 Liston G E, Pielke S R A, Greene E M. Improving first-order snow-related deficiencies in a regional climate model. J Geophys Res, 1999, 104: 19559–19567
94 Rodell M, Houser P R, Jambor U, et al. The global land data assimilation system. Bull Amer Meteor Soc, 2004, 85: 381–394
95 Slater A G, Clark M P. Snow data assimilation via an ensemble Kalman filter. J Hydr, 2006, 7: 478–493
96 Sun C J, Walker J P, Houser P R. A methodology for snow data assimilation in a land surface model. J Geophys Res, 2004, 109: 0148–0227
97 Tedesco M, Kim E J. Intercomparison of electromagnetic models for passive microwave remote sensing of snow. IEEE Trans Geosci Remote Sensing, 2006, 44: 2654–2666
98 Andreadis K M, Lettenmaier D P. Assimilation remotely sensed snow observations into a macroscale hydrology model. Adv Water Resour, 2006, 29: 872–886
99 Durand M, Margulis S A. Feasibility test of multif requency radiometric data assimilation to estimate snow water equivalent. J Hydrometeorol, 2006, 7: 443–457
100 Pulliainen J. Mapping of snow water equivalent and snow depth in boreal and sub-arctic zones by assimilating space-borne microwave radiometer data and ground-based observations. Remote Sens Environ, 2006, 101: 257–269
101 Che T. Passive Microwave Remote Sensing of Snow and Snow Data Assimilation Research. Doctor Thesis. Lanzhou: Cold and Arid Regions Environmental and Engineering Research Institute, 2006. 1–105
102 Nagler T, Rott H. Retrieval of wet snow by means of multitemporal SAR data. IEEE Trans Geosci Remote Sensing, 2000, 38: 754–765
103 Pulliainen J, Engdahl M, Hallikainen M. Feasibility of multitemporal interferometric SAR data for stand-level estimation of boreal forest stem volume. Remote Sens Environ, 2003, 85: 397–409
104 Luojus K, Pulliainen J, Metsamaki S, et al. Accuracy assessment of SAR data-based snow-covered area estimation method. IEEE Trans Geosci Remote Sens, 2006, 44: 277–287
105 Shi J, Dozier J. Mapping seasonal snow with SIR-C/X-SAR in mountainous areas. Remote Sens Environ, 1997, 59: 294–307
106 Shi J, Dozier J, Rott H. Snow mapping in alpine regions with synthetic aperture radar. IEEE Trans Geosci Remote Sensing, 1994, 32: 152–158
107 Strozzi T, Wegmuller U, Matzler C. Mapping wet snow covers with SAR interferometry. Int J Remote Sens, 1999, 12: 2395–2403
108 Shi J, Hensley S, Dozier J. Mapping snow cover with repeat pass synthetic aperture radar. Proceeding of IGARSS, 1997, 2: 628–630
109 Venkataraman G, Singh G, Yamaguchi Y. Fully polarimetric ALOS PALSAR data applications for snow and ice studies. Proceeding of IGARSS, 2010. 1776–1779
110 Longepe N, Shimada M, Allain S, et al. Capabilities of Full-Polarimetric PALSAR/ALOS for Snow Extent Mapping. Proceeding of IGARSS, 2008. 1026–1029
111 Shi J, Dozier J. Inferring snow wetness using C-band data from SIR-C's polarimetric synthetic aperture radar. IEEE Trans Geosci Remote Sensing, 1995, 33: 90–914
112 Ulaby F T, Stiles W H. The active and passive microwave response to snow parameters: 2, Water equivalent of dry snow. J Geophys Res, 1980, 85: 1045–1049
113 Kendra J R, Sarabandi K, Ulaby F T. Radar measurements of snow: Experiment and analysis. IEEE Trans Geosci Remote Sensing, 1998, 36: 864–879
114 Rott H, Matzler C. Possibilities and limits of synthetic aperture radar for snow and glacier surveying. Annals Glaciol, 1987, 9: 195–199
115 Shi J, Dozier J. Estimation of snow water equivalence using SIR-C/X-SAR, part I: Inferring snow density and subsurface properties. IEEE Trans Geosci Remote Sensing, 2000, 38: 2465–2474
116 Shi J, Dozier J. Estimation of snow water equivalence using SIR-C/X-SAR, part II: Inferring snow depth and particle size. IEEE Trans Geosci Remote Sensing, 2000, 38: 2475–2488
117 Shi J, Yueh S, Cline D. On estimation of snow water equivalence using L-band and Ku-band radar. Proc IGRASS, 2003, 2: 845–847
118 Shi J. Estimation of snow water equivalence with two Ku-band dual polarization radar. Proc IGRASS, 2004, 3: 1649–1652
119 Choudhury B J, Schmugge T J, Chang A, et al. Effect of surface roughness on the microwave emission from soil. J Geophys Res, 1979, 84: 5699–5706
120 Wang J R, O'Neill P E, Jackson T J, et al. Multifrequency measurements of the effects of soil moisture, soil texture, and surface roughness. IEEE Trans Geosci Remote Sensing, 1983, 21: 44–51
121 Shi J, Chen K S, Li Q, et al. A parameterized Surface Reflectivity Model and Estimation of Bare Surface Soil Moisture with L-band Radiometer. IEEE Trans Geosci Remote Sensing, 2002, 40: 2674–2686
122 Njoku E G, Li L. Retrieval of land surface parameters using passive microwave measurements at 6–18 GHz. IEEE Trans Geosci Remote Sensing, 1999, 37: 79–93
123 Liou Y A, Liu S F, Wang W J. Retrieving soil moisture from simulated brightness temperatures by a neural network. IEEE Trans Geosci Remote Sensing, 2001, 39: 1662–1672
124 Frate D, Ferrazzoli F P, Schiavon G. Retrieving soil moisture and agricultural variables by microwave radiometry using neural networks. Remote Sens Environ, 2003, 84: 174–183
125 Liu S F, Liou Y A, Wang W J, et al. Retrieval of crop biomass and soil moisture from measured 1.4 and 10.65 GHz brightness temperatures. IEEE Trans Geosci Remote Sensing, 2000, 40: 1260–1268
126 Dubois P C, Van Zyl J J, Engman E T. Measuring soil moisture with imaging radar. IEEE Trans Geosci Remote Sensing, 1995, 33: 195–926
127 Shi J, Wang J, Hsu A, et al. Estimation of bare surface soil moisture and surface roughness parameters using L-band SAR image data.

IEEE Trans Geosci Remote Sensing, 1997, 35: 1254–1266
128 Oh Y, Sarabandi K, Ulaby F T. An empirical model and inversion technique for radar scattering from bare soil surface. IEEE Trans Geosci Remote Sensing, 1992, 30: 370–381
129 Shi J, Chen K S. Estimation of Bare Surface Soil Moisture with L-band Multi-polarization Radar Measurements. Proc IGRASS, 2005. 2191–2194
130 Jackson T J, Schmugge T J. Vegetation effects on the microwave emission of soils. Remote Sens Environ, 1991, 36: 203–212
131 Prevot L, Champion I. Estimating surface soil moisture and leaf area index of a wheat canopy using a dual-frequency (C and X bands) Scatterometer. Remote Sens Environ, 1993, 46: 331–339
132 Freeman A, Durden S L. A three-component scattering model for polarimetric SAR data. IEEE Trans Geosci Remote Sensing, 1998, 36: 963–973
133 Du J Y, Shi J. The development of HJ SAR soil moisture retrieval Algorithm. Int J Remote Sens, 2010, 31: 3691–3705
134 Lee K H, Anagnostou E N. A combined passive/active microwave remote sensing approach for surface variable retrieval using Tropical Rainfall Measuring Mission observations. Remote Sens Environ, 2004, 92: 112–125
135 O'Neill P E, Chauhan N S, Jackson T J. Use of active and passive microwave remote sensing for soil moisture estimation through corn. Int J Remote Sens, 1996, 17: 1851–1865
136 Njoku E N, Wukson W J, Dinardo S J, et al. Observation of soil moisture using a passive and active low-Frequency microwave airborne sensor during SGP99. IEEE Trans Geosci Remote Sensing, 2002, 40: 2659–2671
137 Narayan U, Lakshmi V, Jackson T J. High-resolution change estimation of soil moisture using L-band radiometer and radar observations made during the SMEX02 experiments. IEEE Trans Geosci Remote Sensing, 2006, 44: 1545–1554
138 Das N N, Entekhabi D, Njoku E G. An Algorithm for merging SMAP radiometer and radar data for high resolution soil moisture retrieval. IEEE Trans Geosci Remote Sensing, 2011, 49: 1504–1512
139 Mcfarland M J, Miller R L, Christopher M. Land surface temperature derived from the SSM/I passive microwave brightness temperature. IEEE Trans Geosci Remote Sensing, 1990, 28: 839–845
140 Mao K B, Shi J, Li Z L, et al. A physics-based statistical algorithm for retrieving land surface temperature from AMSR-E passive microwave data. Sci China Ser D-Earth Sci, 2007, 50: 1115–1120
141 Mao K B, Shi J, Tang H J, et al. A neural –network technique for retrieving land surface temperature from AMSR-E passive microwave data. Proc IGRASS, 2007, 7: 4422–4425
142 Choudhury B J, Tucker C J, Golus R E, et al. Monitoring vegetation using nimbus-7 scanning multichannel microwave radiometers data. Int J Remote Sens, 1987, 8: 533–538
143 Choudhury B J, Tucker C J. Monitoring global vegetation using Nimbus-7 37 GHz data: Some empirical relations. Int J Remote Sens, 1987, 8: 1085–1090
144 Pampaloni P, Paloscia S, Zipoli G. Microwave emission of soil and vegetation at X and Ka bands. Proc IGRASS, 1983. 900–905
145 Wang J R. Effect of vegetation on soil moisture sensing observed from orbiting microwave radiometers. Remote Sens Environ, 1985, 17: 141–151
146 Paloscia S, Pampaloni P. Microwave polarization index for monitoring vegetation growth. IEEE Trans Geosci Remote Sensing, 1988, 26: 617–621
147 Paloscia S, Pampaloni P. Microwave vegetation indexes for detecting biomass and water conditions of agricultural crops. Remote Sens Environ, 1992, 40: 15–26
148 Griend A A, Owe M. Microwave vegetation optical depth and inverse modelling. Meteorol Atmosph Phys, 1994, 54: 225–239
149 Shi J, Jackson T, Tao J, et al. Microwave vegetation indices for short vegetation covers from satellite passive microwave sensor AMSR-E. Remote Sens Environ, 2008, 112: 4285–4300
150 LeVine D M, Karam M A. Dependence of attenuation in a vegetation canopy on frequency and plant water content. IEEE Trans Geosci Remote Sensing, 1996, 34: 1090–1096
151 Kerr Y H, Njoku E N. A semiempirical model for interpreting microwave emission from semiarid land surfaces as seen from space. IEEE Trans Geosci Remote Sensing, 1990, 28: 384–393
152 Becker F, Choudhury B J. Relative sensitivity of normalized difference vegetation Index (NDVI) and microwave polarization difference Index (MPDI) for vegetation and desertification monitoring. Remote Sens Environ, 1988, 24: 297–311
153 Njoku E G, Chan T K. Vegetation and surface roughness effects on AMSR-E land observations. Remote Sens Environ, 2006, 100: 190–199
154 Min Q, Lin B. Remote sensing of evapotranspiration and carbon uptake at Harvard forest. Remote Sens Environ, 2006, 100: 379–387
155 Chen L, Shi J, Wigneron J P. The Development of Microwave Vegetation Index for Future SMOS Applications. Proc IGRASS, 2009. 89–92
156 Sahoo A K, Houser P R, Ferguson C, et al. Evaluation of AMSR-E soil moisture results using the *in-situ* data over the Little River Experimental Watershed, Georgia. Remote Sens Environ, 2008, 112: 3142–3152
157 Wigneron J P, Chanzy A, Calvet J C, et al. A simple algorithm to retrieve soil moisture and vegetation biomass using passive microwave measurements over crop fields. Remote Sens Environ, 1995, 51: 331–341
158 Chai L, Shi J, Zhang L, et al. A parameterized microwave model for short vegetation layer. Proceeding of IGRASS, 2010. 2023–2026
159 Zhang N, Shi J, Sun G, et al. Assessment of Boreal Forest Biomass using L-Band Radiometer SMOS Data. Proceeding of IGARSS, 2011. 1946–1949
160 Cimino J, Brandani A, Casey D, et al. Multiple incidence angle SIR-B experiment over Argentina: Mapping of forest units. IEEE Trans Geosci Remote Sensing, 1986, 4: 498–509
161 Ranson K J, Sun G Q. Mapping biomass of a northern forest using multifrequency SAR data. IEEE Trans Geosci Remote Sensing, 1994, 32: 388–396
162 Pierce L E, Ulaby F T, Sarabandi K, et al. Knowledge-based classification of polarimetric SAR images. IEEE Trans Geosci Remote Sensing, 1994, 32: 1081–1086
163 Rignot E J M, Williams C L, Way J, et al. Mapping of forest types in Alaskan boreal forests using SAR imagery. IEEE Trans Geosci Remote Sensing, 1994, 32: 1051–1059
164 Saatchi S S, Rignot E. Classification of boreal forest cover types using SAR images. Remote Sens Environ, 1997, 60: 270–281
165 Saatchi S S, Soares J V, Alves D S. Mapping deforestation and land use in Amazon rainforest by using SIR-C imagery. Remote Sens Environ, 1997, 59: 191–202
166 Simard M, Saatchi S S, De G G. The use of decision tree and multiscale texture for classification of JERS-1 SAR data over tropical forest. IEEE Trans Geosci Remote Sensing, 2000, 38: 2310–2321
167 Lee J S, Grunes M R, Pottier E, et al. Unsupervised terrain classification preserving polarimetric scattering characteristics. IEEE Trans Geosci Remote Sensing, 2004, 42: 722–731
168 Cloude S R, Pottier E. An entropy based classification scheme for land applications of polarimetric SAR. IEEE Trans Geosci Remote Sensing, 1997, 35: 68–78
169 Lee J S, Grunes M R, Pottier E. Quantitative comparison of classification capability: fully polarimetric versus dual and single-polarization SAR. IEEE Trans Geosci Remote Sensing, 2001, 39: 2343–2351
170 Shimoni M, Borghys D, Heremans R, et al. Fusion of PolSAR and PolInSAR data for land cover classification. Inter J Appl Earth Obser Geoinform, 2009, 11: 169–180
171 Lardeux C, Frison P L, Tison C, et al. Support vector machine for multifrequency SAR polarimetric data classification. IEEE Trans Geosci Remote Sensing, 2009, 47: 4143–4152
172 Sánchez-Lladó F J, Pajares G, Gonzalo P, et al. Improving the wishart synthetic aperture radar image classifications through deterministic simulated annealing. ISPRS-J Photogramm Remote Sens, 2011, 66: 845–857
173 Entezari I, Homayouni S, Homayouni M, et al. Classification of po-

larimetric SAR images using Support Vector Machines. Can J Remote Sens , 2011, 10: 011–029
174 Mishra P, Singh D, Yamaguchi Y. Land cover classification of palsar images by knowledge based decision tree classifier and supervised classifiers based on SAR observables. Prog Electromagn Res, 2011, 30: 47–70
175 Haddadi G A, Sahebi M R, Ali M. Polarimetric SAR feature selection using a genetic algorithm. Can J Remote Sens, 2011, 37: 27–36
176 Qi Z, Yeh A G, Xia L, et al. A novel algorithm for land use and land cover classification using RADARSAT-2 polarimetric SAR data. Remote Sens Environ, 2012, 118: 21–39
177 Toan L, Beaudoin A, Riom J, et al. Relating forest biomass to SAR data. IEEE Trans Geosci Remote Sensing, 1992, 30: 403–411
178 Dobson M C, Ulaby F T, Letoan T, et al. Dependence of radar backscatter on coniferous forest biomass. IEEE Trans Geosci Remote Sensing, 1992, 30: 412–415
179 Beaudoin A, Letoan T, Goze S, et al. Retrieval of forest biomass from SAR data. Int J Remote Sens, 1994, 15: 2777–2796
180 Rignot E, Way J B, Williams C, et al. Radar estimates of aboveground biomass in boreal forests of interior Alaska. IEEE Trans Geosci Remote Sensing, 1994, 32: 1117–1124
181 Harrell P A, Bourgeau-Chavez L L, Kasischke E S, et al. Sensitivity of ERS-1 and JERS-1 radar data to biomass and stand structure in Alaskan boreal forest. Remote Sens Environ, 1995, 54: 247–260
182 Imhoff M L. A theoretical-analysis of the effect of forest structure on synthetic-sperture radar backscatter and the remote-sensing of biomass. IEEE Trans Geosci Remote Sensing, 1995, 33: 341–352
183 Kasischke E S, Christensen N L, Bourgeau-Chavez L L. Correlating radar backscatter with components of biomass in Loblolly-Pine forests. IEEE Trans Geosci Remote Sensing, 1995, 33: 643–659
184 Pulliainen J T, Mikkela P J, Hallikainen M T, et al. Seasonal dynamics of C-band backscatter of boreal forests with applications to biomass and soil moisture estimation. IEEE Trans Geosci Remote Sensing, 1996, 34: 758–770
185 Foody G M, Green R M, Lucas R M, et al. Observations on the relationship between SIR-C radar backscatter and the biomass of regenerating tropical forests. Int J Remote Sens, 1997, 18: 687–694
186 Harrell A, Kasischke E S, Bourgeau-Chavez L L, et al. Evaluation of approaches to estimating aboveground biomass in southern pine forests using SIR-C data. Remote Sens Environ, 1997, 59: 223–233
187 Ranson K J, Sun G, Weishampel J F, et al. Forest biomass from combined ecosystem and radar backscatter modeling. Remote Sens Environ, 1997, 59: 118–133
188 Ranson K J, Sun G. Effects of environmental conditions on boreal forest classification and biomass estimates with SAR. IEEE Trans Geosci Remote Sensing, 2000, 38: 1242–1252
189 Sun G, Ranson K J, Kharuk V I. Radiometric slope correction for forest biomass estimation from SAR data in the Western Sayani Mountains, Siberia. Remote Sens Environ, 2002, 79: 279–287
190 Kimes D S, Ranson K J, Sun G. Inversion of a forest backscatter model using neural networks. Int J Remote Sens, 1997, 18: 2181–2199
191 Frate D F, Solimini D. On neural network algorithms for retrieving forest biomass from SAR data. IEEE Trans Geosci Remote Sensing Lett, 2004, 42: 24–34
192 Ni W. Forest Biomass Retrieval Based on 3D Radar Backscattering Model Using PALSAR Data. Doctoral Desertation, Beijing: Graduate University of Chinese Academey of Sciences, 2009
193 Luckman A, Baker J, Wegmuller U. Repeat-pass interferometric coherence measurements of disturbed tropical forest from JERS and ERS satellites. Remote Sens Environ, 2000, 73: 350–360
194 Gaveau D L A. Modelling the dynamics of ERS-1/2 coherence with increasing woody biomass over boreal forests. Int J Remote Sens, 2002, 23: 3879–3885
195 Santoro M , Askne J, Smith G, et al. Stem volume retrieval in boreal forests from ERS-1/2 interferometry. Remote Sens Environ, 2002, 81: 19–35
196 Santoro M, Shvidenko A, McCallum I, et al. Properties of ERS-1/2 coherence in the Siberian boreal forest and implications for stem volume retrieval. Remote Sens Environ, 2007, 106: 154–172
197 Hagberg J O, Ulander L M H, Askne J. Repeat-pass SAR interferometry over forested terrain. IEEE Trans Geosci Remote Sensing, 1995, 33: 331–340
198 Pang Y, Li Z Y. InSAR technology and its application to estimate stand average height (in Chinese). J Remote Sensing, 2003, 7: 8–13
199 Cloude S R, Papathanassiou K P. Polarimetric SAR interferometry. IEEE Trans Geosci Remote Sensing, 1998, 36: 1551–1565
200 Papathanassiou K P, Cloude S R. Single-baseline polarimetric SAR interferometry. IEEE Trans Geosci Remote Sensing, 2001, 39: 2352–2363
201 Cloude S R, Papathanassiou K P. Three-stage inversion process for polarimetric SAR interferometry. IEEE Proc Radar Sonar Navigation, 2003, 150: 125–134
202 Yamada H, Yamaguchi Y, Rodriguez E, et al. Polarimetric SAR interferometry for forest canopy analysis by using the super-resolution method. IEEE Geoscience and Remote Sensing Symposium, 2001. 1101–1103
203 Yamada H, Sato K, Yamaguchi Y, et al. Interferometric phase and coherence of forest estimated by ESPRIT-based polarimetric SAR interferometry. IEEE Geoscience and Remote Sensing Symposium, 2002. 829–831
204 Cloude S R. Polarization coherence tomography. Radio Sci, 2006, 41: 1–27
205 Paloscia S. An empirical approach to estimating leaf area index from multifrequency SAR data. I Int J Remote Sens, 1998, 19: 359–364
206 Manninen T, Stenberg P, Rautiainen M, et al. Leaf area index estimation of boreal forest using ENVISAT ASAR. IEEE Trans Geosci Remote Sensing, 2005, 43: 2627–2635
207 Chen J, Lin H, Huang C D, et al. The relationship between the leaf area index (LAI) of rice and the C−band SAR vertical/horizontal (VV/HH) polarization ratio. Int J Remote Sens, 2009, 30: 2149–2154